NASA/CR–2014-218156

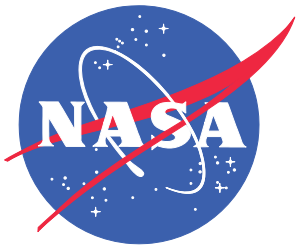

Cyclic Crack Growth Testing of an A.O. Smith Multilayer Pressure Vessel with Modal Acoustic Emission Monitoring and Data Assessment

Steven M. Ziola
Digital Wave Corporation, Centennial, Colorado

January 2014

NASA STI Program . . . in Profile

Since its founding, NASA has been dedicated to the advancement of aeronautics and space science. The NASA scientific and technical information (STI) program plays a key part in helping NASA maintain this important role.

The NASA STI program operates under the auspices of the Agency Chief Information Officer. It collects, organizes, provides for archiving, and disseminates NASA's STI. The NASA STI program provides access to the NASA Aeronautics and Space Database and its public interface, the NASA Technical Report Server, thus providing one of the largest collections of aeronautical and space science STI in the world. Results are published in both non-NASA channels and by NASA in the NASA STI Report Series, which includes the following report types:

- TECHNICAL PUBLICATION. Reports of completed research or a major significant phase of research that present the results of NASA Programs and include extensive data or theoretical analysis. Includes compilations of significant scientific and technical data and information deemed to be of continuing reference value. NASA counterpart of peer-reviewed formal professional papers, but having less stringent limitations on manuscript length and extent of graphic presentations.

- TECHNICAL MEMORANDUM. Scientific and technical findings that are preliminary or of specialized interest, e.g., quick release reports, working papers, and bibliographies that contain minimal annotation. Does not contain extensive analysis.

- CONTRACTOR REPORT. Scientific and technical findings by NASA-sponsored contractors and grantees.

- CONFERENCE PUBLICATION. Collected papers from scientific and technical conferences, symposia, seminars, or other meetings sponsored or co-sponsored by NASA.

- SPECIAL PUBLICATION. Scientific, technical, or historical information from NASA programs, projects, and missions, often concerned with subjects having substantial public interest.

- TECHNICAL TRANSLATION. English-language translations of foreign scientific and technical material pertinent to NASA's mission.

Specialized services also include organizing and publishing research results, distributing specialized research announcements and feeds, providing information desk and personal search support, and enabling data exchange services.

For more information about the NASA STI program, see the following:

- Access the NASA STI program home page at *http://www.sti.nasa.gov*

- E-mail your question to help@sti.nasa.gov

- Fax your question to the NASA STI Information Desk at 443-757-5803

- Phone the NASA STI Information Desk at 443-757-5802

- Write to:
  STI Information Desk
  NASA Center for AeroSpace Information
  7115 Standard Drive
  Hanover, MD 21076-1320

NASA/CR–2014-218156

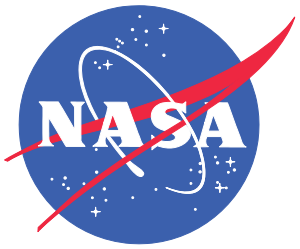

Cyclic Crack Growth Testing of an A.O. Smith Multilayer Pressure Vessel with Modal Acoustic Emission Monitoring and Data Assessment

Steven M. Ziola
Digital Wave Corporation, Centennial, Colorado

National Aeronautics and
Space Administration

Langley Research Center
Hampton, Virginia 23681-2199

Prepared for Langley Research Center
under Contract NNA09DB39C

January 2014

Available from:

NASA Center for AeroSpace Information
7115 Standard Drive
Hanover, MD 21076-1320
443-757-5802

Executive Summary

Digital Wave Corp. (DWC) was retained by Jacobs ATOM at NASA Ames Research Center to perform cyclic pressure crack growth sensitivity testing on a multilayer pressure vessel instrumented with DWC's Modal Acoustic Emission (MAE) system, with captured wave analysis to be performed using DWCs WaveExplorer™ software, which has been used at Ames since 2001 [Refs. 13 - 15]. The objectives were to document the ability to detect and characterize a known growing crack in such a vessel using only MAE, to establish the sensitivity of the equipment vs. crack size and / or relevance in a realistic field environment, and to obtain fracture toughness materials properties in follow up testing to enable accurate crack growth analysis. Although the wave propagation theory and acoustic science behind MAE is well established, no prior crack-correlation validation testing of this nature had been attempted on multilayer vessels, which exhibit significant noise emissions under loading and which are thicker walled with tougher material than the vessels on which the method was originally validated. From DWC's own prior work and that of others, such as documented in Ref. 10 by Southwest Research Institute (SwRI), it was also known that stable crack growth does not emit strong AE signals, and they likely would not become so until the crack was near critical size. Using toughness properties provided by NASA from work performed in 1975 [Ref. 11], it was believed that the crack induced in this vessel would be closer to critical size than, in fact, it was based on later material property testing and analysis by SwRI [Ref 9] that revealed the shell material to be much tougher than originally indicated by NASA.

Crack growth starter notches were milled into the outer shell layer of a surplus A.O. Smith multilayer pressure vessel obtained from Kennedy Space Center, serial number MV50466-8. The vessel was pressure cycled 4,688 times at stress levels between 1/2 of yield and nominal yield strength of the shell material. A visible crack indication was seen in the center-shell crack under a video magnifier after about two thousand cycles, but its depth could not be determined during testing. No clear MAE signals were obtained real-time during this phase of crack growth, but some were revealed in later examination. Due to funding limitations, the test was ultimately terminated when several cycles of yield-level stress were applied to force crack extension. It was later determined in post-processing that a low level MAE crack signal was captured during these final cycles. In general, the MAE response was less than anticipated, and it is possible that this crack, if hidden, would not have been identified with a normal test level-of-effort. However, the refinements in filtering made possible by this test will improve future field assessments, although the sensitivity and crack size correlation to signal strength were not clearly established since the crack was at the threshold of detectability for this tough material. Future cyclic testing should focus on welds and weld heat affected zone which are more likely to crack in service, and are also more likely to emit strong AE signals assuming they are lower toughness material.

The vessel was subsequently sent to Southwest Research Institute (SwRI) on a subcontract for fractographic analysis of the center crack and for testing of strength, fracture toughness, and fatigue crack growth properties to facilitate correlation of the actual crack with fracture mechanics calculations, which were reported in Ref. 7. This materials testing work demonstrated that the crack grew 0.064 inches before the final, rapid through-wall extension under yield level stress, and provided extensive fracture toughness data. The photomicrographs also showed that the crack growth was not uniform across the crack front, and was highly plastic, which also had an unanticipated negative effect on the ability to identify the crack using MAE because of the

more diffuse plastic energy release mechanism. In retrospect, a smaller, elastic mode crack extension may have been easier to detect. Nonetheless, the filtering developed to evaluate these results will significantly improve the data assessments in future testing.

Revision 1 of this test report is issued to incorporate findings from Phase 2 materials testing performed by SwRI [Ref. 9] and to make various editorial changes, more complete reference citations in the text, and typographical corrections.

Table of Contents

List of Figures

List of Tables

Section 1. Testing Outline and Objectives

The objective of this testing was to determine whether non-critical fatigue crack growth detection in an actual, previously in-service, non-ASME Code multi-layered pressure vessel under realistic cyclic pressure loading was possible using modal acoustic emission (MAE) waveform assessment methodology, and to attempt to determine the sensitivity limits of such detection. It has been demonstrated unequivocally that energy releases from Pentel 2H 0.3 mm lead breaks (as per ASTM E-1419) can be detected for ranges well over 20 feet from inner and outer surfaces and from intermediate layers of these vessels, and was done so again in this test. However, it is believed that the energy from the lead breaks is so large it is useful only to establish the presence of a large growing crack, likely near-critical size. In order to improve the usefulness of the MAE method for fitness for service and life extension, a more detailed understanding is required of the actual crack sizes (sub-critical) that can be detected in the presence of the considerable non-relevant noise in tests of these vessels (due to layer wash at welds, corrosion flakes breaking, layer relative movement, etc.). Towards this end, the following steps were taken.

1. NASA provided the test vessel to be used for testing, A. O. Smith pressure vessel, MV50466-8, which was located at the Kennedy Space Center facility. This vessel and a backup were shipped by DWC to our Centennial, CO headquarters. To ensure safe operations, a bunker was excavated in the soil in the back field area such that the vessel was entirely below the surface, and the trench walls were reinforced with wood and a roof cover was constructed. This also protected the vessel from the elements, and minimized nonrelevant environmental noise sources.
2. The vessel was prepped for fatigue testing and monitoring using Digital Wave Corporation's WaveExplorerTM waveform analysis modal acoustic emission data acquisition hardware and software analysis techniques.
3. Preparation and pre-inspection for safety assessment included x-ray inspection of the head-to-shell welds, magnetic particle inspection of the outer long seam weld, and borescope inspection of the internal geometry of the head-to-shell welds. There were no unacceptable defects identified.
    a. The vessel outer diameter was also measured to 0.001" accuracy at both zero and 6600 psi pressure in accordance with ASME Section VIII, Div 1, part ULW to assess the extent of gaps between layers.
    b. A one-inch diameter part-through hole was machined through 7 of the 12 shell layers in order to provide accessible intermediate layer surfaces for performing lead break calibrations and coupling studies.
4. Axial flaws were machined by a milling cutter into the vessel near both head-to-shell welds, and at the center of the vessel. Due to schedule and budget limitations as well as physical constraints with the vessel, a more precise EDM notch could not be applied.
5. Strain gages were mounted on the vessel head, near the head-to-shell weld and at the center of the vessel to monitor the strain during the cycling and to be able to correlate actual stresses experienced to theoretical, given the potential for gaps in the layers.
6. The vessel was then hydrostatically cycled to induce flaw growth at the notches.

Test Objectives

1. Document the ability to detect modal acoustic emission events from fatigue crack growth under realistic field testing condition
2. Monitor strain readings during the cyclic testing to ensure that the vessel was not plastically deforming and to have strain data if stress calculations need to be performed at a later date.
3. Perform fractographic analysis of the crack growth and ASTM tensile, fracture toughness, stress intensity and fatigue crack growth (da/dn) testing of the material properties of the vessel.
4. Correlate actual measured incremental crack growth with MAE signals to establish energy release sensitivity and nonrelevant noise discrimination in order to improve multilayer pressure vessel structural integrity assessments using the MAE waveform assessment methodology.

Section 2. A.O. Smith Pressure Vessel and Vessel Preparation

Figure 1 shows the drawing of A. O. Smith pressure vessel MV50466-8, used in the testing. The vessel consisted of 11 layers of approximately 0.25 inch thick wraps, with a 0.375 inch thick liner (12 total layers). This resulted in a vessel with an approximate wall thickness of 3.125 inches, a 30 inch ID, and a 36.25 inch OD. The spherical head wall thickness was a minimum of 2.5 inches.

Figure 2 shows a picture of the cross section of the head-to-shell weld of the vessel that was obtained by SwRI after the vessel was sectioned, Ref [7]. In the photograph the layers of the vessel can be clearly seen. Except for the outer layer in this small section of the vessel, the layers are in intimate contact when the vessel is in use, which was also demonstrated by the measured stress levels and diameter expansion measurements. Because the wavelengths of the plate waves are so long, they do not interact with the layers, unlike typical frequencies used in ultrasonic inspections. This was also separately verified and documented in testing performed by DWC at ARC in 2001 and 2002 [Refs. 13 and 14].

The nameplate is shown in Figure 3, and contains pertinent information about the vessel.

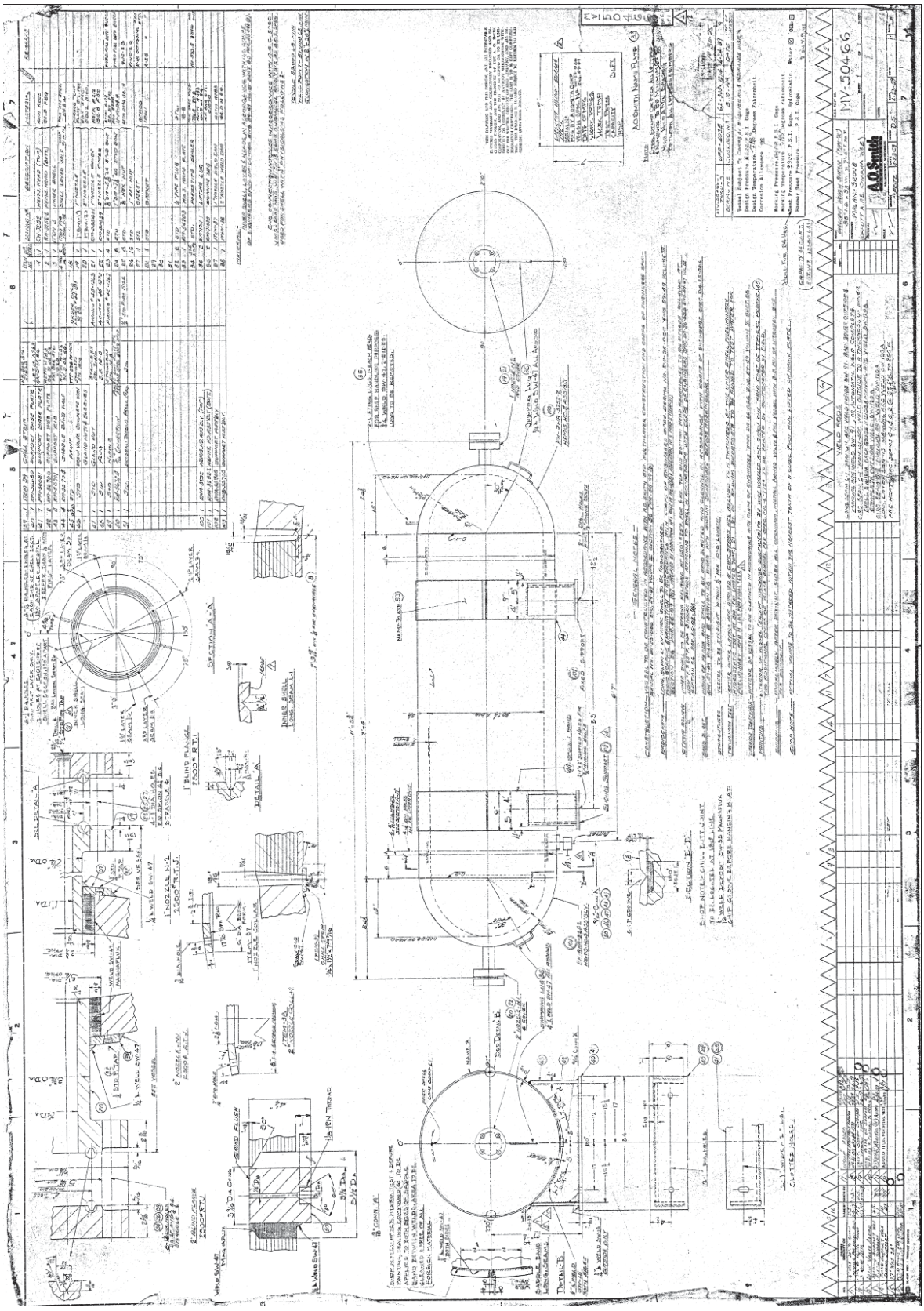

Figure 1 - Drawing of A. O. Smith MV50466-8 pressure vessel.

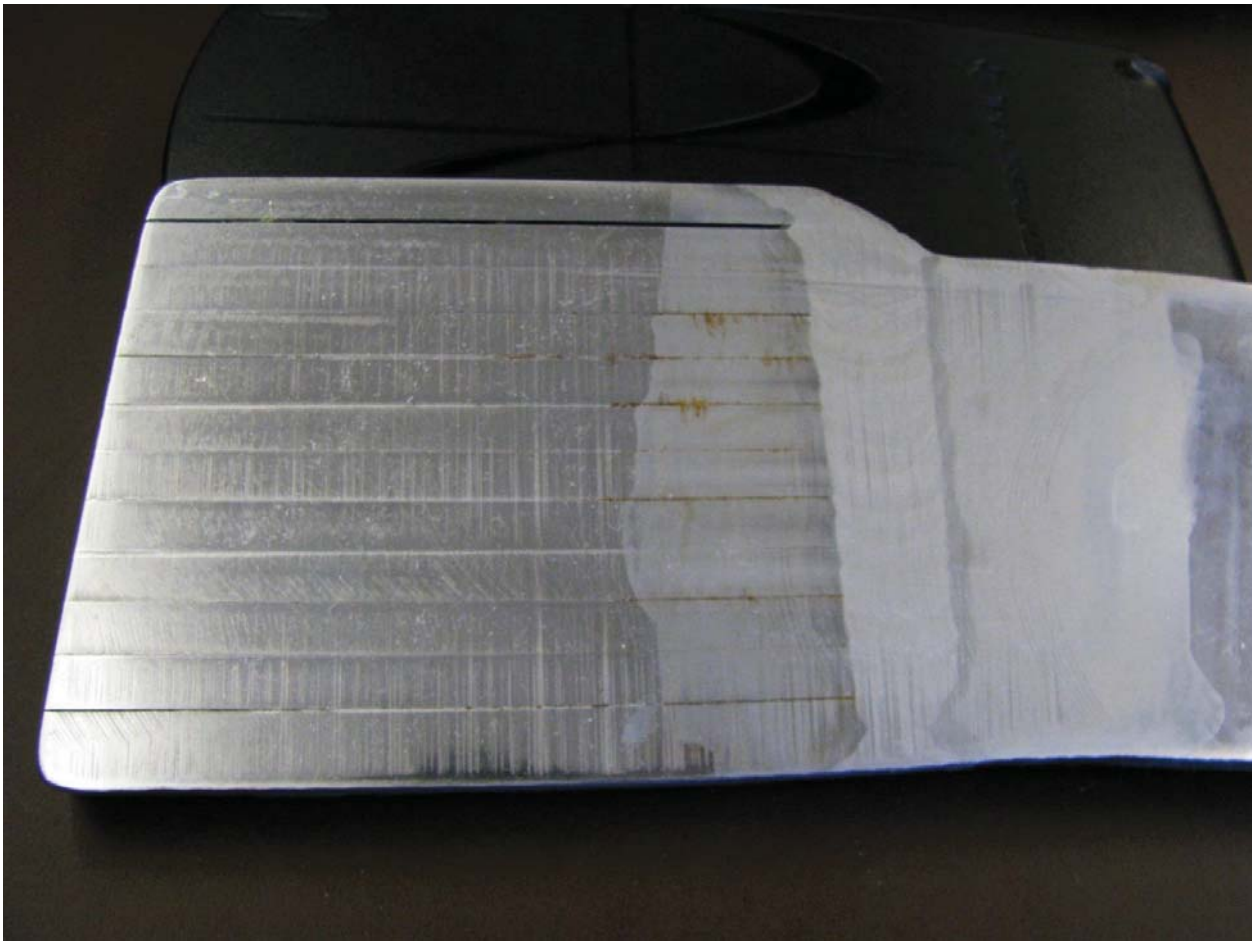

Figure 2 - Cross section of the head to shell weld of the A. O. Smith pressure vessel MV50466-8 (section provided by SwRI)

The eleven one-quarter inch layers and the single three-eighths inch inner layer can be clearly seen in the photo. This sample was prepared after the cycling was finished and while the metallurgical analysis was being performed. Other samples showed that he gap between the outer layers was a local artifact, and not representative of the entire vessel.

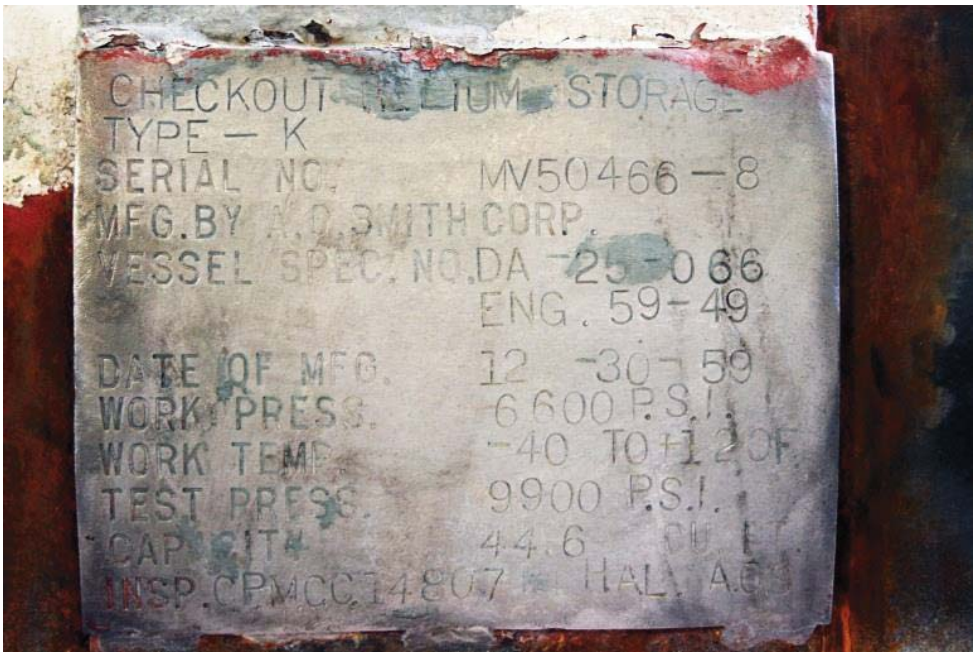

Figure 3 - Nameplate on the MV50466 A. O. Smith pressure vessel

Flaws were machined into the vessel using a 6 inch diameter, 60^0 milling cutter. This was done on a large milling machine, Figure 4.


Figure 4 - Milling of the flaws into the vessel.

Longitudinal flaws were machined at both ends 0.5 inches in from the edge of the head-to-shell welds, and one in the center of the vessel. All flaws were inline, at the top of the vessel, due to the constraints of the mill.

The flaws were machined to a depth of 0.175 inches into the outer wrap, and by using the large diameter cutter created a radiused notch in the outer layer, approximately 2 inches long. Electro discharge machining for the notches was considered, but due to the short time frame to get the testing started, it was not possible to find a vendor that could machine the notches in the time frame needed.

Figure 5 below shows a montage of pictures as the vessel was prepped for testing.

Figure 5 - Vessel Preparation for Testing

This grouping of pictures above shows the preparation of the vessel for the fatigue testing. Starting at the upper left and going clockwise shows, the cutter and the notch; the relationship of the notch to the edge of the head-to-shell weld; the hole drilled into the side of the vessel through seven layers; the seven layers numbered by layer, the vessel (the hole can be seen at the right side of the vessel); and the length of the notch (this is the notch at the center of the vessel).

Section 3. Testing Instrumentation and Hardware

Strain Gages and Strain Instrumentation

Strain gages were mounted on the vessel to provide strain readings on the vessel spherical head, head-to-shell weld and at the center of the weld. Figure 6 shows the gages on the head and the head-to-shell weld. National Instruments strain gage instrumentation was used to perform these measurements. The strain gages used were from Micro-measurements. The gages were wired using a three wire configuration to account for wire resistance.

Strain Gages: Micro-measurements strain rosette, CEA-06-125UR-120
Strain Gage Instrumentation: National Instruments cDAQ-9181 CompactDAQ 1-slot Ethernet chassis connected to a National Instruments 9235 8-channel quarter-bridge strain gage module. System control was done through a National Instruments USB-6008 12-bit, 10 kS/s multifunction DAQ module.

Figure 6 - Strain gages mounted on the head and near the head-to-shell weld of the vessel

The National Instruments system was capable of 8 channels of acquisition. Since the strain field at the center of the vessel should be well described by classical thin wall pressure vessel theory, only the axial and hoop gages were acquired (not the 45^0). All three of the gages on the head and head-to-shell strain gage rosettes were acquired so that the full strain field could be calculated, if needed.

Figures 7-9 show close-ups of all the strain gages.

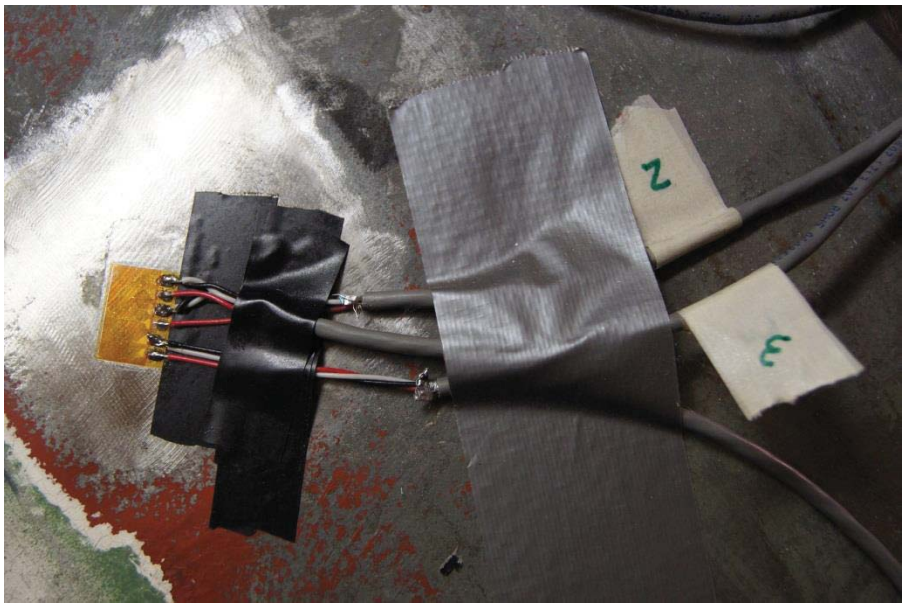

Figure 7 - Strain gage mounted on the vessel head

This photograph shows the strain gage mounted on the head of the vessel. The gage was a triaxial gage, with one gage along the axial direction, one along the circumferential direction and one at 45^0.

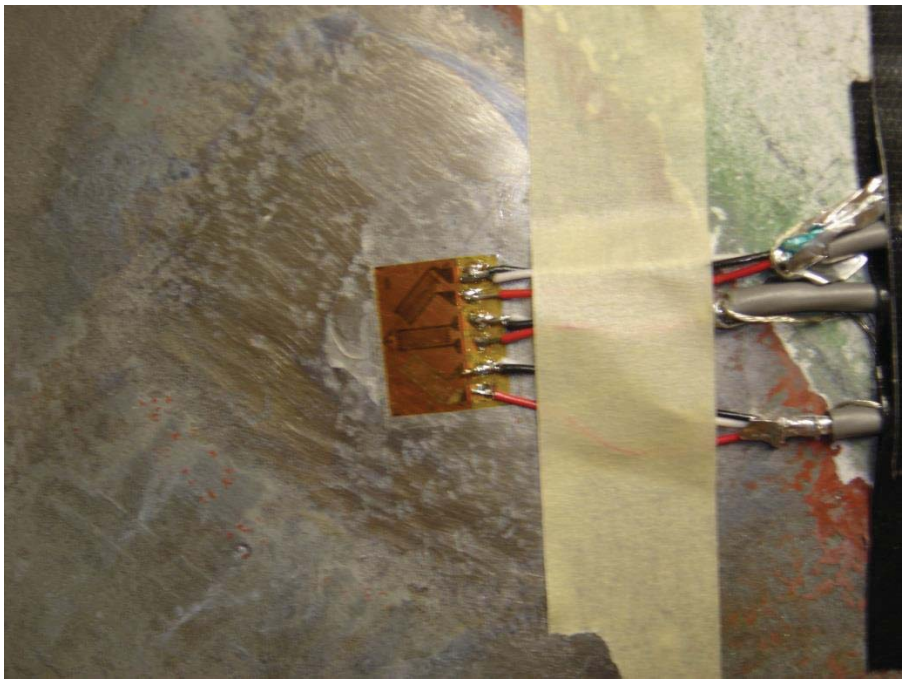
Figure 8 - Strain gages at the head-to-shell weld location

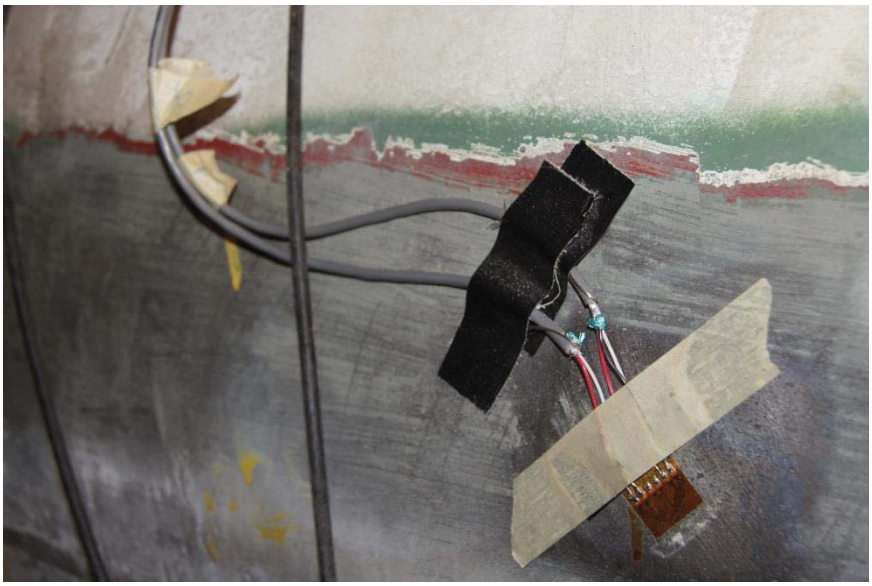

Figure 9 - Strain gages mounted at the center of the vessel

Modal Acoustic Emission Instrumentation

The instrumentation used for the monitoring of the cyclic test vessel was the Digital Wave Corporation WaveExplorer™ MAE system, Figure 10. This is a broadband system with full high-speed wave capture. It has been proven capable and qualified for measuring multilayer pressure vessels through work done at several NASA research centers, as well as for retesting and requalification of DOT containers (for example, see DWC's DOT Special Permit 15332, Ref. 12). The exact components used for the tests are given below.

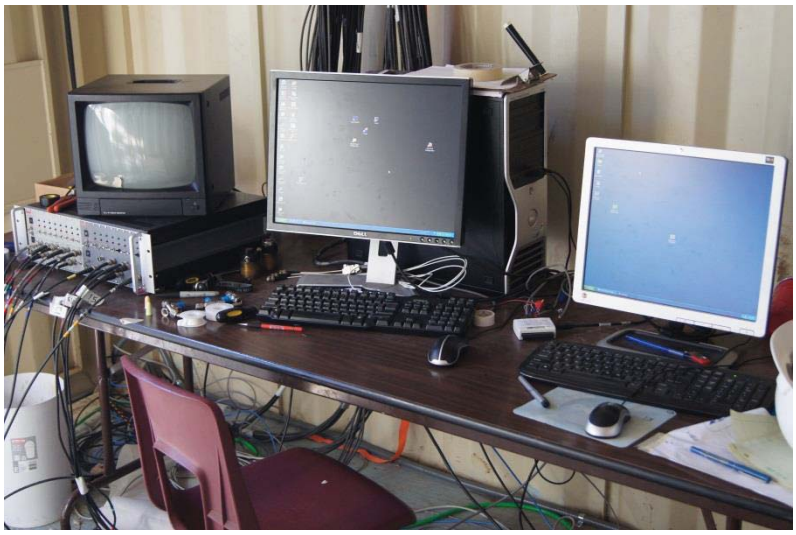

Figure 10 - MAE Equipment Setup

This photograph shows the FM1, video microscope monitor (on top of the FM1), and the monitors for the modal AE and pump control and pressure and strain data acquisition. The

settings shown here for the filters are for the analog portion of the hardware. Values shown in Appendix C are for the software digital filters.

Hardware
Sensors: Digital Wave B225-5 IPP
Preamplifiers: Digital Wave P20
Signal Conditioning: Digital Wave FM1

Software
Data Acquisition: Digital Wave WaveExplorer™ software
Data Acqusition System Settings
A/D Rate: 2MHz
Total System Gain: 68 dB
Highpass Filter: 20 kHz
Lowpass Filter: 750 kHz
Points per Waveform: 4096
Pretrigger Points: 1024

The MAE system threshold used for the tests was 32 dB_{AE}. This threshold is specified in ASTM E 1419 [Ref. 16], and has been generally shown to be adequate for AE testing, although ASTM E 1419 itself is only applicable to seamless single layer vessels. Further assessment of this parameter will be performed based on the results of this test on a multilayer vessel. That the -02b edition referenced above is cited as mandatory in DWC's DOT special permit for cylinder requalification, Ref. 12.

Cyclic Pressurization of A. O. Smith Vessel

The pumps used for the testing were pneumatically operated, high pressure pumps. These pumps are relatively robust and inexpensive, and are typically used for hydraulic pressurization of high pressure bottles. Each system was fitted with high pressure stainless steel tubing and fittings, a mechanical gage, and a 0-10 volt pressure transducer so that pressure readings could be digitized and stored for each mechanical and MAE test. Pressure transducers were calibrated against the mechanical gage for each pressure system. An infrared temperature transducer was also incorporated into each pressure system so that water temperature could be monitored, digitized and stored. The components in each system are listed below.

0-10,000 psi Cyclic Pressurization:

Pump:	*Pressure Gage:*	*Pressure Transducer:*	*Temperature Transducer:*
Haskel Model #: GSF-60 Pressure Range: 7500 psi	ENFM Pressure Range: 0-10,000 psi	WIKAI Model #: A-10 Pressure Range: 0-10,000 psi Voltage Range: 0-10 volts	Omega Model #: OS 136-1-V Temperature Range: 0-400^0 F Voltage Range: 0-10 volts

14,000 psi Pressurization:

Pump:	*Pressure Gage:*	*Pressure Transducer:*	*Temperature Transducer:*
Sprague Products, Curtiss-Wright Flow Control Group Model #: S216J300 P/N: 77895-51001 Pressure Range: 33,500 psi	McDaniel Controls, Model G, 30,000 psi	Omegadyne Inc. Model #: PX02S1-30KG10T Pressure Range: 0-30,000 psi Voltage Range: 0-10 volts	Omega Model #: OS 136-1-V Temperature Range: 0-400^0 F Voltage Range: 0-10 volts

Section 4. Pressure and Strain Data

Representative strain data is shown in the Figures 11-13 below. The first set of three figures show the strain readings for a 0-7260 psi pressure cycle. The vessel was rated by A.O. Smith for a pressure of 6600 psi, with a factor of safety of 2 on yield stress. It can be seen from these plots that the strain remained linear throughout the cycle, and thus no plastic deformation is occurring.

The next set of Figures 14-16 shows the pressure-strain curves for the 14,000 psi load (2.2 over operating pressure). It can be seen from these plots that at this pressure, the vessel began to deform plastically, as the strain began to roll over. This is clearly seen in the shell plots.

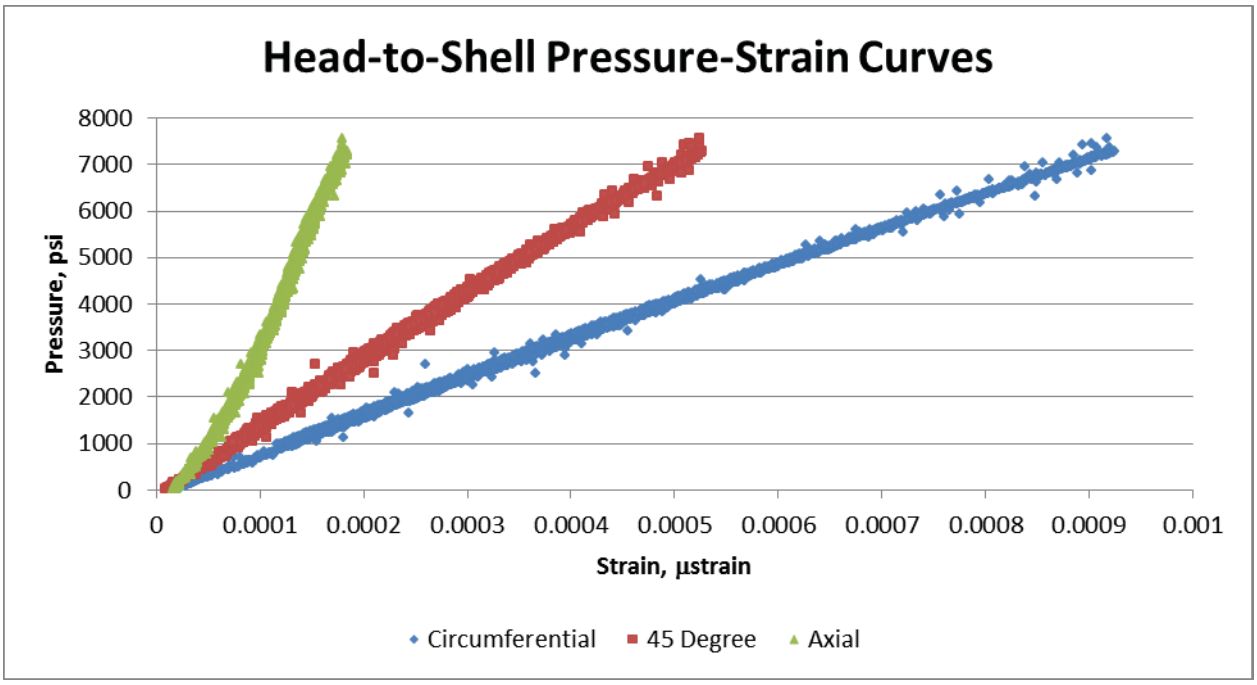

Figure 11 - Strain vs. Pressure, 7260 psig, head-to-shell weld

Figure 11 shows the strain readings for the circumferential (hoop), 45^0 and axial strains for a pressurization of 7260 psi for the strain gages mounted at the head-to-shell weld.

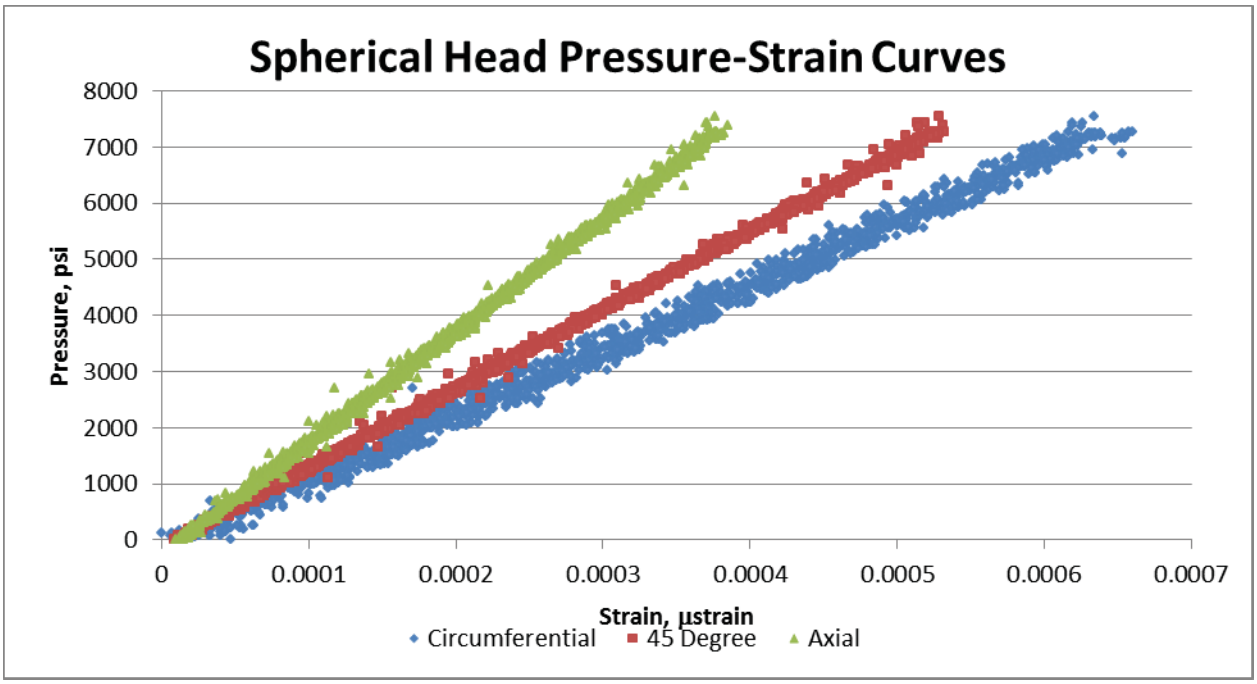

Figure 12 - Strain vs. Pressure, 7260 psig, spherical head

Figure 12 shows the strain readings for the circumferential (hoop), 45^0 and axial strains for a pressurization of 7260 psi for the strain gages mounted on the spherical head.

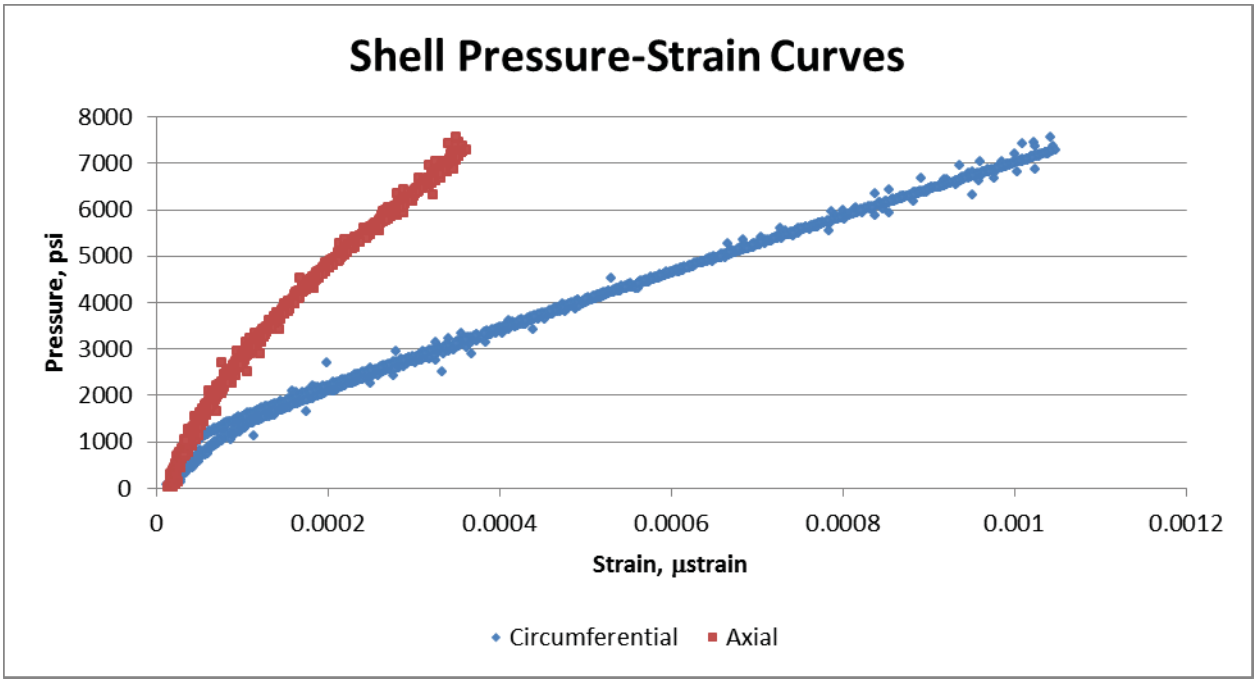

Figure 13 - Strain vs. pressure, 7260 psig, shell center

This plot (Figure 13) shows the strain readings for the circumferential (hoop), and axial strains for a pressurization of 7260 psi for the strain gages mounted on the shell at the center of the vessel.

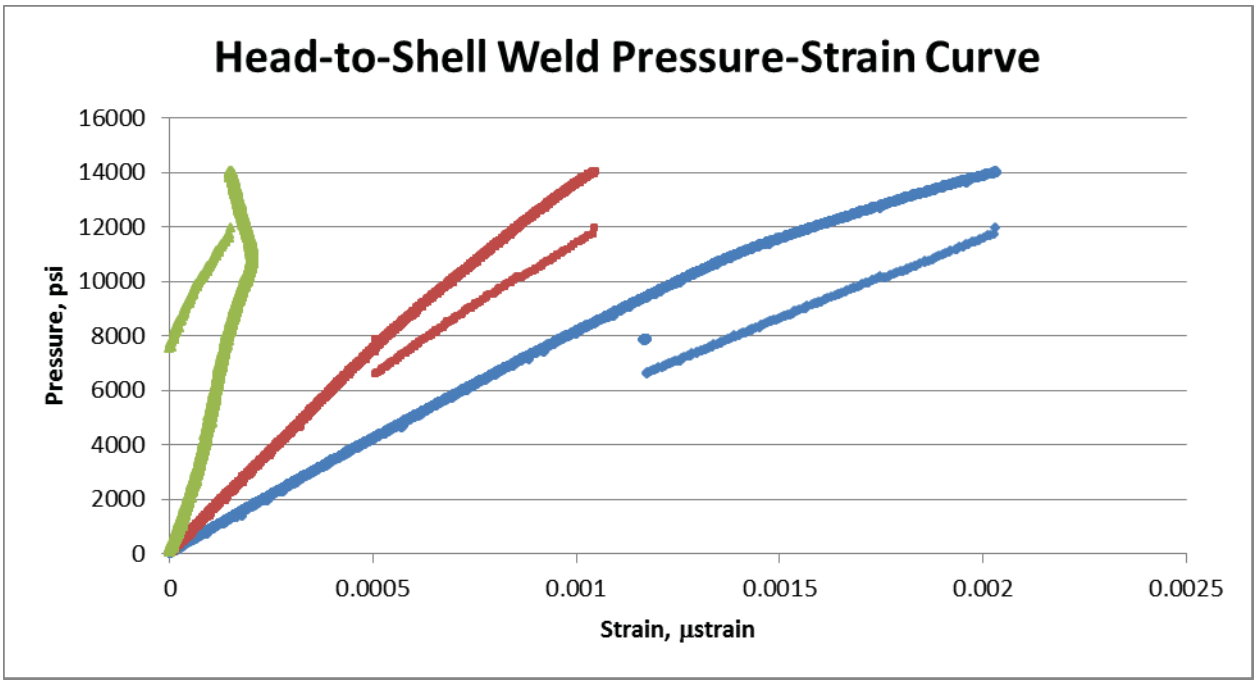

Figure 14 - Strain vs. Pressure, 14,000 psig, head-to-shell weld

Figure 14 shows the strain readings for the circumferential (hoop), 45^0 and axial strains for a pressurization of 14,000 psi for the strain gages mounted at the head-to-shell weld. The data below each of the pressure-strain plots is the offset in the strain due to the plastic deformation of the vessel.

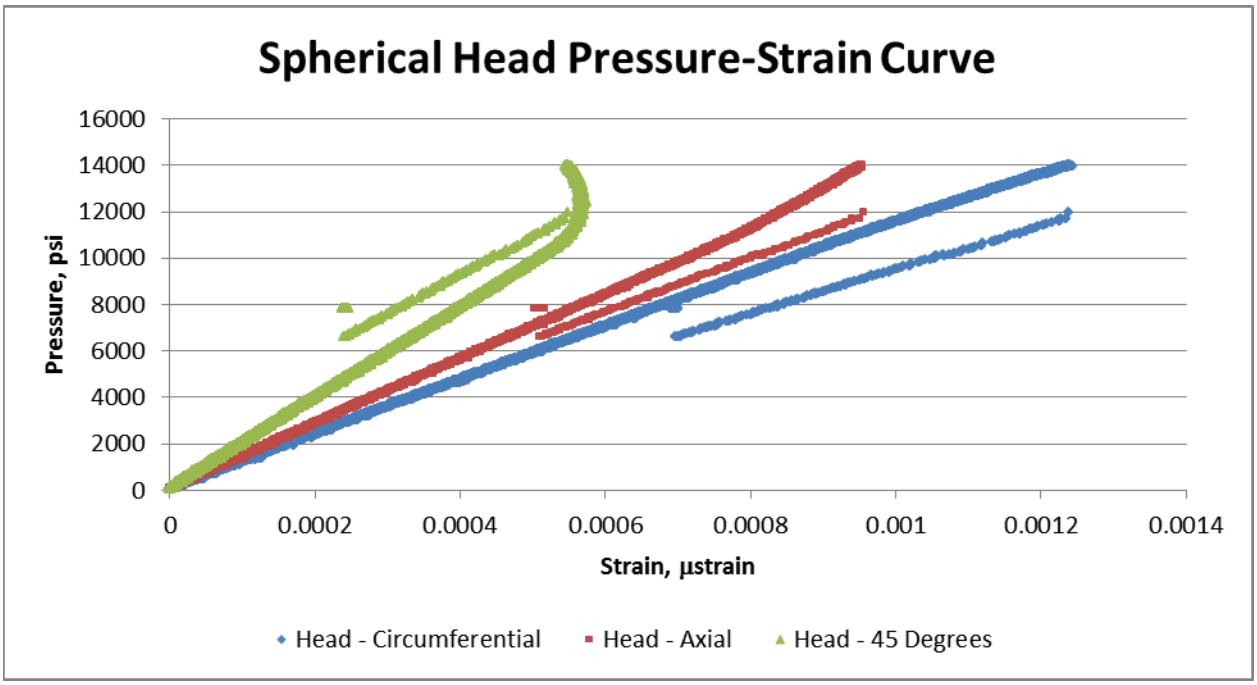

Figure 15 - Strain vs. Pressure, 14,000 psi, spherical head

Figure 15 shows the strain readings for the circumferential (hoop), 45^0 and axial strains for a pressurization of 14,000 psi for the strain gages mounted on the spherical head.

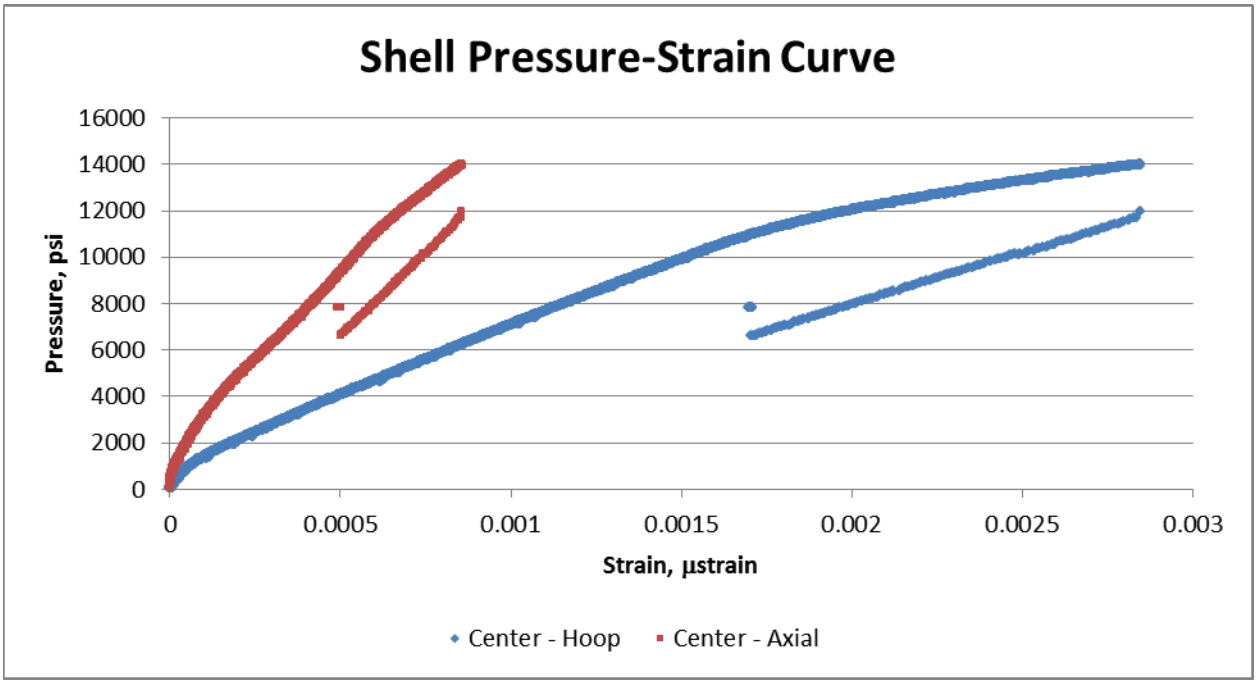

Figure 16 - Strain vs. Pressure, 14,000 psig, center of vessel

This plot shows the strain readings for the circumferential (hoop) and axial strains for a pressurization of 14,000 psi for the strain gages mounted on the shell at the center of the vessel.

Figure 17, below, shows the cyclic pressurization plot for 12/28/2011, for cycles from 1000-8400 psi. This is shown as a representative example of the cycling performed. All test files have the pressurization files digitized and stored in electronic format. The maximum and minimum cycling pressures used for each days testing are shown in the table in Appendix A. Table of Test Files.

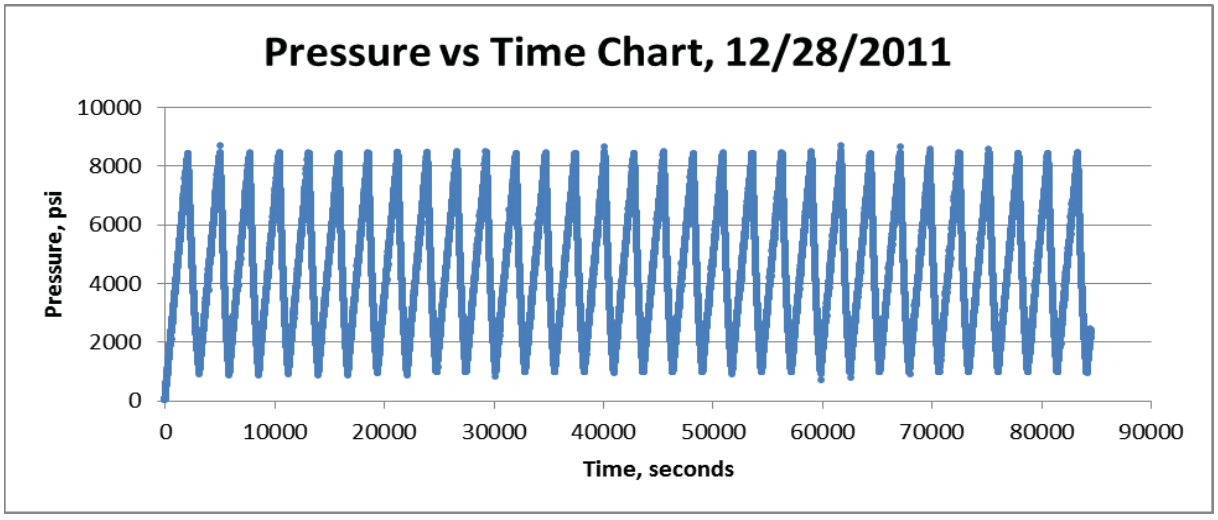

Figure 17 - Cyclic pressurization cycles for 1000-8400 psi.

Section 5. Modal Acoustic Emission – Review, Theory and Practice

Historical Review of Conventional Acoustic Emission Analysis for Pressure Vessels

For much of the history of acoustic emission testing, it was thought that the wave propagation due to flaw growth in structures was too complicated to understand. This led to parameter based analysis techniques, such as scatter plots of amplitude, duration, counts, and other single parameter analyses. The first mistake in this approach is thinking that these are independent parameters – they are not. If this is thought of in terms of a bell, if the bell is struck hard, a long (duration) and loud (amplitude) tone will result, and vice versa. Correlating these two against each other does not provide unique information about the bell. This, noise and flaw growth discrimination is not be possible with this approach.

However, even with this limitation, AE had useful qualities. The main one was that event locations could be remotely determined. By measuring the difference in arrival times of the wave at two or more sensors, the location of the event could be calculated. This was taken advantage of in the testing of DOT high strength tube trailer cylinders. The low mechanical noise environment of this testing, combined with the ability to perform ultrasonic examination for flaw characterization, eliminated the need for source characterization through analysis of the AE results, and the analysis was reduced to determining the given number of events at a single location. Specifically, if five events were located in the same location, then follow-up ultrasonic inspection was required to verify the flaw and flaw size. This test method was developed in the early 1980's by Blackburn and Rana, Ref. 1, and then ASTM E 1419 was written around this work. This work also set the threshold sensitivity of the AE systems (32 dB_{AE}) for the detection of flaws in these high strength steel pressure vessels. This sensitivity could be used with the existing equipment available at that time (early 1980's), because there were no interfaces in the tubes to create noise or to prevent ultrasonic inspection, and the systems were filtered to remove signal frequencies below 100 kHz and above 300 kHz (narrowband filtering). Thus, event rates were low, and the equipment could process the data without saturating. Plus, determination of flaw existence was done with a follow-up method, e.g., ultrasound. Thus, the false calls typically associated with AE could be eliminated.

However, in moving on to multi-layered vessels, this approach breaks down. Why? Because of the way that multi-layered vessels are manufactured, when they are pressurized they emit significant amounts of noise over the entire length of the vessel. As pressurization occurs, the layers rub against each other, as well as weld slag and other impurities, and create noise sources. Tens of thousands of events per cycle, at the 32 dB_{AE} threshold, are not unusual. Parameter based approaches will not work, and source location will not discriminate possible relevant flaw growth events from non-relevant noise in this environment. More sophisticated analysis techniques are required to sort these large numbers of events at the 32 dB_{AE} threshold setting.

In conventional AE around this time, "expert systems" were developed to perform the analysis of AE data on structures that did require source discrimination. Dr. Timothy Fowler of the Monsanto Corporation approached fiberglass tank failures by creating an acoustic emission database of signal parameters from tanks that he had tested, and then visually inspected to determine if they were good or bad. AE signal parameters from follow-on tests were compared against the information in the database, and then rated the tanks from good to "failed". This

approach was highly successful for Monsanto since the database correlated directly to the tanks under test, and there were a large number of these tanks. However, using this database to analyze data from high pressure vessels would result in the passing of bad vessels, and the failure of good vessels. Why? Because the database was developed for atmospheric tanks that had large mechanical failure sources, such as mixers, that caused large events. In this case, large energy events were bad. If we look at the failure mechanism in high pressure/high strength steel vessels, the large amplitude/large energy failure assumption is most definitely **not** the case unless a crack is already at critical size. Pressure vessels in almost all common services fail by fatigue crack growth. If one looks at the energy release in this mechanism for the very ductile, tough steels in use in these vessels, it is very small in the stable fatigue crack growth regime. In this case, small amplitude, high frequency events, with specific wave modes are "bad" events, and large amplitude events are typically from events not related to flaw growth, and are usually caused by rubbing of supports or fracturing of brittle corrosion products.

While acoustic emission has always held promise, due to its remote monitoring capabilities, it was historically plagued by its inability to sort noise source from true flaw growth. This is due to the simplistic nature of many of the analysis approaches that have been taken in this field due to the lack of wave propagation knowledge of the practitioners. Blindly applying non-applicable criteria will result in false calls. If a database approach is used, the analysis in the database must be known and understood in order to for the user to determine whether the analysis is truly analyzing the vessel under test with the correct physics. Analysis techniques, when possible, must be based on well understood engineering principles, and be able to withstand an engineering audit. If not, a false sense of security is created, and the safety goals cannot be met.

Overview of Modal Acoustic Emission

Modal AE analysis is based on well documented ultrasonic wave modes that propagate in engineering structures [2 - 3]. The analysis is very similar to that of seismology, where primary waves (p-waves) and secondary waves (s-waves) are analyzed to determine the source type, magnitude and location of earthquakes. In plate-like structures (for purposes of MAE analysis, pressure vessels are rolled-up plates) the wave modes of interest are the extensional mode (in-plane stretching and compressing of the plate) and the flexural mode (bending of the plate).

Source Orientation Discrimination

When a defect (e.g., a crack) grows it has depth (it is not a surface source) into the vessel wall, and it releases its energy into the plane of the wall, and creates a propagating extensional mode (compression-tension motion). Sources such as corrosion and rust on the exterior surface of the vessel, or vessels contacting each other, release the energy out of the plane of the plate, and cause the plate to bend (much like striking the head of a drum) as the wave propagates. This source type creates large flexural modes. The two modes have very distinct characteristics (see the figures below), and can be identified. They also have different propagation velocities that can be accurately predicted from acoustic dispersion curves for a given plate.

Noise Identification and Rejection

By analyzing mode shapes, the source can be more readily identified with MAE than with conventional AE techniques that use qualitative analyses to try to identify sources. This is important since this approach has the potential to eliminate the false calls that are so familiar in conventional AE testing.

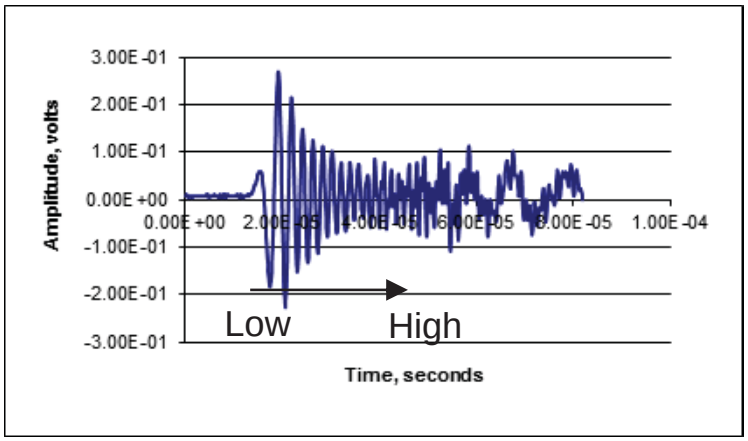

Frequency goes from low to high

Figure 18 - Extensional Mode

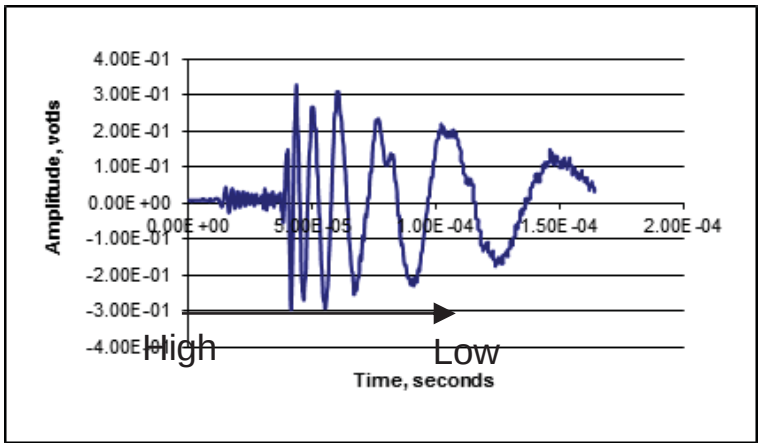

Frequency goes from high to low

Figure 19 - Flexural Mode

Theoretical Predictions

Since Modal AE is based on first principles, theoretical predictions can be made prior to testing to guide the tester in analyzing the data. Figures 20 and 21 below show the theoretical predictions using DWC's WavePredictor^{TM} software for the experimental data shown in Figures 18 and 19 above.

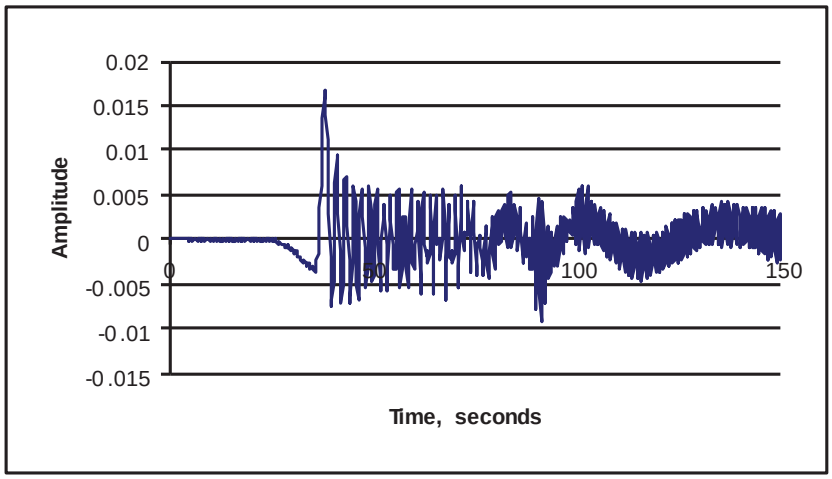

Figure 20 - Theoretically extensional mode

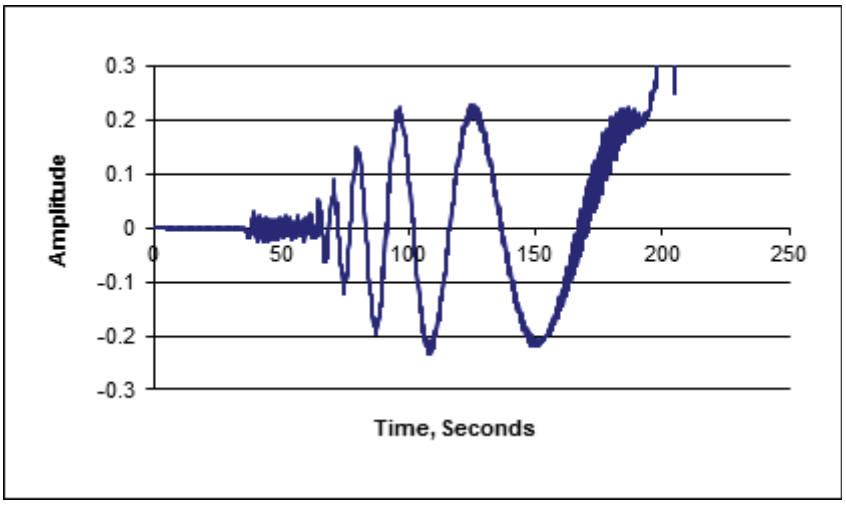

Figure 21 - Theoretically predicted flexural mode

As stated above, Modal AE analyzes the wave modes produced by the source orientation and material geometry to detect flaw growth. Conventional AE (e.g., MONPAC™) uses simplified parameter-based analyses, based on parameters obtained from resonant sensors such as signal duration, amplitude, hit-counts, and energy. These parameters are not unique parameters for a given source. As Dr. Goranson, former Chief of Structures at Boeing states in [5], "***"Classical" AE data consist of various parameters intended to represent the AE waveform. The parameters characterizing a given waveform are not necessarily unique to that waveform and could be the same for other waves generated by other types of sources.***" Thus, it is very difficult to characterize various signals according to their source if the parameter approach is taken. Furthermore, in conventional AE, the signal (waveform) is not stored and the only information the tester is left with is a few parameters stripped from the signal - with no wave mode or frequency content information available. Even if the signal were to be stored, the mode information is lost due to the resonant sensor and narrowband filtering inherent in these systems.

Another approach that has come into use, capturing the waves digitally but then categorizing them using such classical parameters as amplitude, duration, energy and counts by stripping the

information from the wave, is also not modal acoustic emission testing or assessment because the wave shape and frequency content are still not considered. The approach taken in this testing was true Modal AE as described above.

Section 6. Fatigue Testing of the A. O. Smith Vessel and MAE Results

MAE Sensor Locations

Fifteen sensors were arrayed on the vessel. Two array configurations were used, and are shown In Figures 22 and 23. At cycle 3292 the sensor from the heads were moved onto the shell to aid in source location at the center notch. Appendix A has the date, file name and cycle information listed.

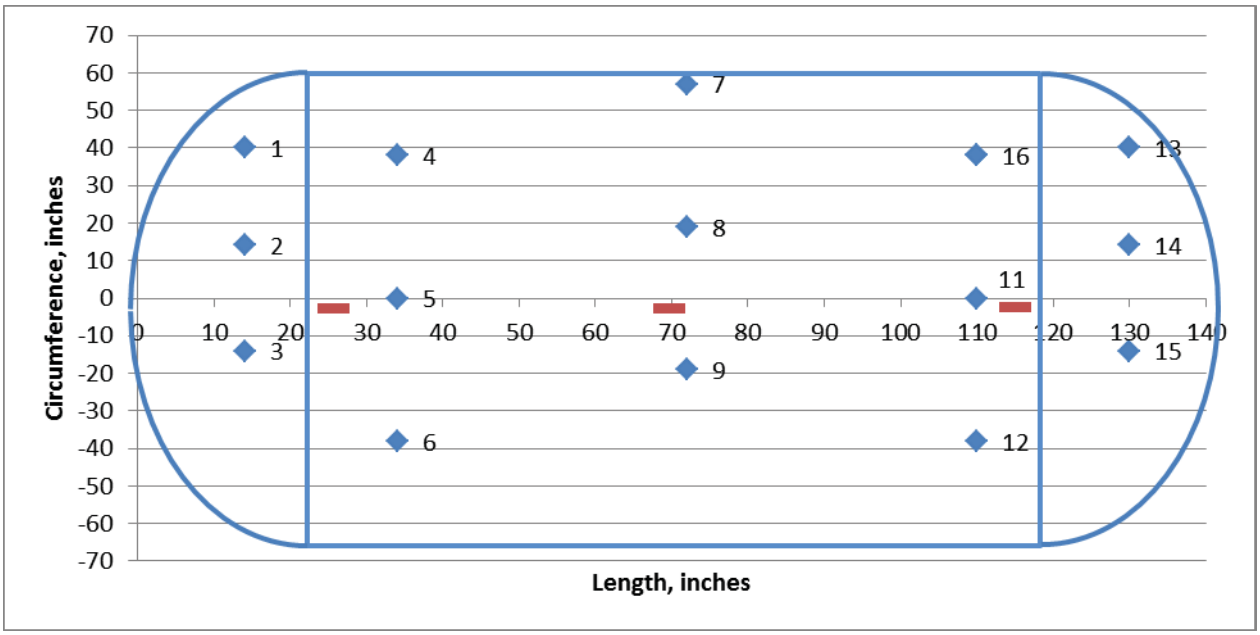

Figure 22 - Sensor locations for cycles 1 - 3291

Notch locations are shown as red dashes. The rough outline of the unwrapped vessel is shown. The top of the vessel is at y = 0, and the bottom of the vessel is at approximately +/-60 inches.

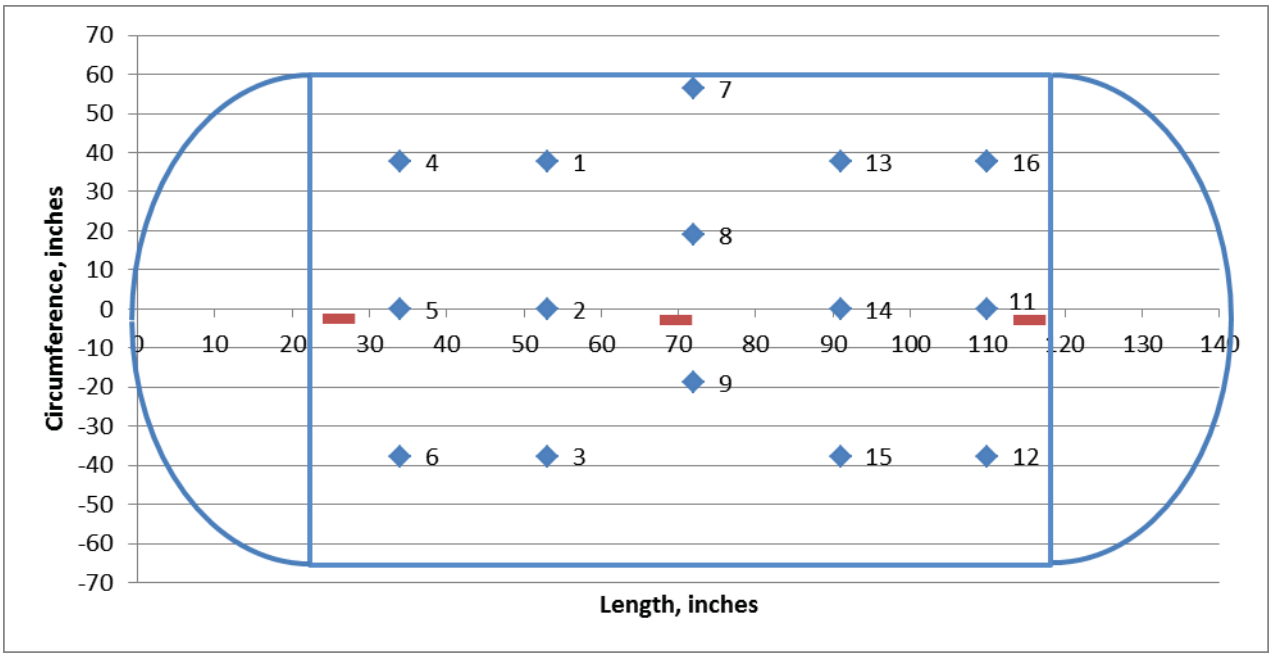

Figure 23 - Sensor locations for cycles 3292 - 4688

Notch locations are shown as red dashes. The rough outline of the unwrapped vessel is shown. The top of the vessel is at y = 0, and the bottom of the vessel is at approximately +/-60 inches.

Fracture Mechanics

Crack Growth Rates

From NASA Technical Memorandum X-3316, December 1975 [Ref 11], the da/dN curve for the A. O. Smith vessel steel was claimed to be represented by the classical Paris equation with the following constants:

Rearranging gives: $\frac{da}{dN} = (3.6x10^{-10})(\Delta K)^3$

Integrating this equation results in: $N = \int_{a_i}^{a_f} \frac{da}{3.6\times10^{-10}\left[M\Delta\sigma\sqrt{\pi a}\right]^3}$

$$a_f = \left[\frac{1}{a_i^{-0.5} - (0.5)(3.6\times10^{-10})(M^3\Delta\sigma^3\pi^{1.5}\Delta N)}\right]^2$$

Assuming an elliptical crack (Barsom, Ref 6, with *M*=1, and a flaw depth of 0.175 inches and an operating stress of 35.2 ksi gives the following curve, Figure 24, for the crack growth per cycle.

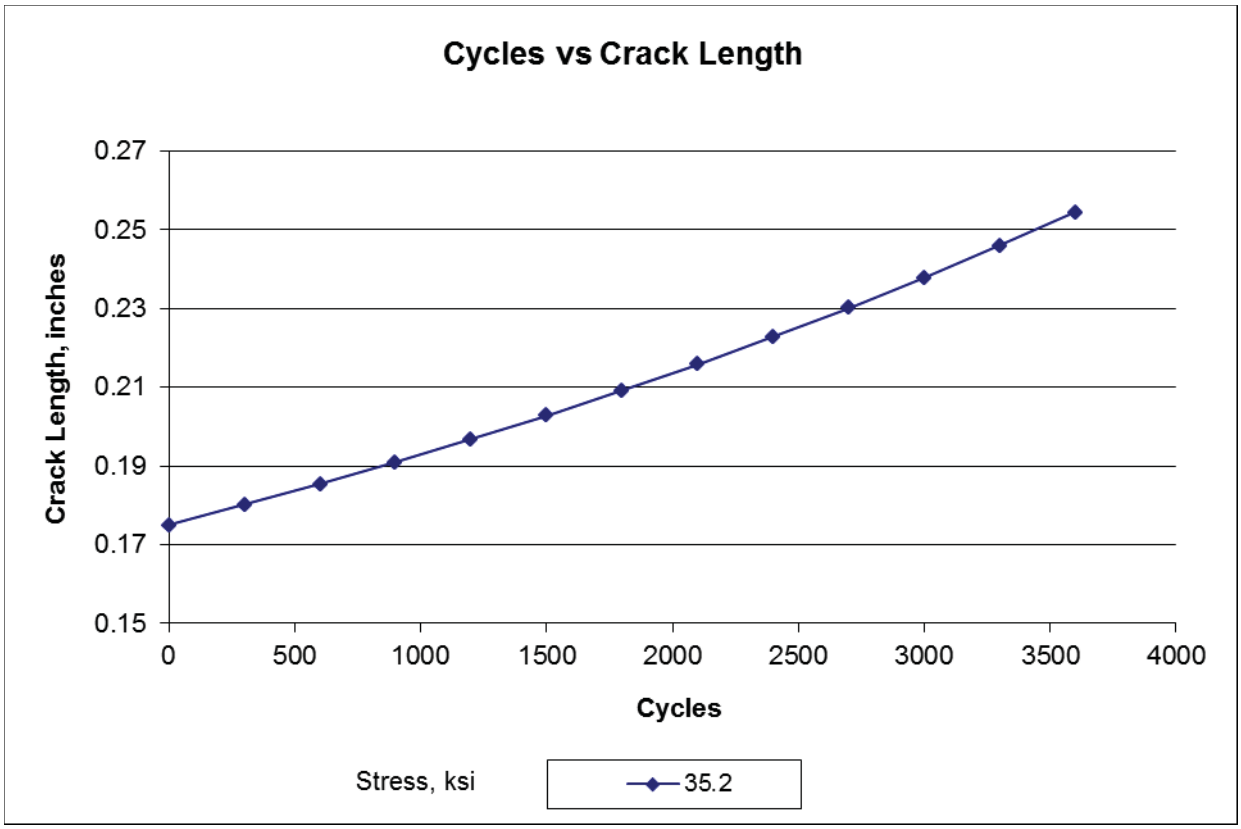

Figure 24 - da/dN curve based on data from NASA Technical Memorandum X-3316 [Ref 11]

The crack depth used in this analysis was chosen based on the initial three month test time. Assuming 30 cycles per day (based on the rate of pressurization of the pump), this would result in approximately 900 cycles per month. Over this time frame (2700 cycles), and an initial crack depth of 0.175 inches, the crack would grow approximately 0.055 inches over this time frame. Since the referenced 1975 NASA report identified the critical toughness for the shell material to be about 80 ksi√inch, which was also approximately the applied ΔK during this test, it was felt that enough fracture of the shell layer wall should occur to produce unambiguous MAE events above the threshold setting. Subsequent SwRI material testing proved that the actual critical fracture toughness was much higher (in the range of 170 ksi√inch, Ref [9], and hence that the crack was still in the stable crack growth regime when the test was terminated. Therefore, the actual low level emissions captured and evaluated on reanalysis were consistent with results from prior experience.

Crack Growth Sensitivity

Using the analysis outlined in Appendix B, it was calculated that the crack growth per cycle, due to the cyclic fatigue loading, would produce events of sufficient energy to be detected for the given sensor spacing. However, this assessment was based on elastic energy release for lower toughness material rather than elastic-plastic as was determined to be the actual case, and the Appendix B assessment was not shown to be applicable in the data obtained. Further work is needed in this area.

Pencil Lead Breaks (PLB's)

Pencil lead breaks (Pentel 2H 0.3 mm) were performed inside each of the notches. This was done for several reasons, which are listed below.

1. To see if all the sensors were coupled and had similar detection sensitivities.
2. To see if the wave modes were being developed as expected.
3. To see if the location accuracy of the PLB source could be maintained.

Wave Mode Formation

Below is a representative waveform, Figure 25, from a lead break at the center notch. Channel 8 has been expanded to show the mode formation more clearly. From this the extensional and flexural modes can be observed forming, thus the plate wave analysis will be suitable for this vessel for source identification.

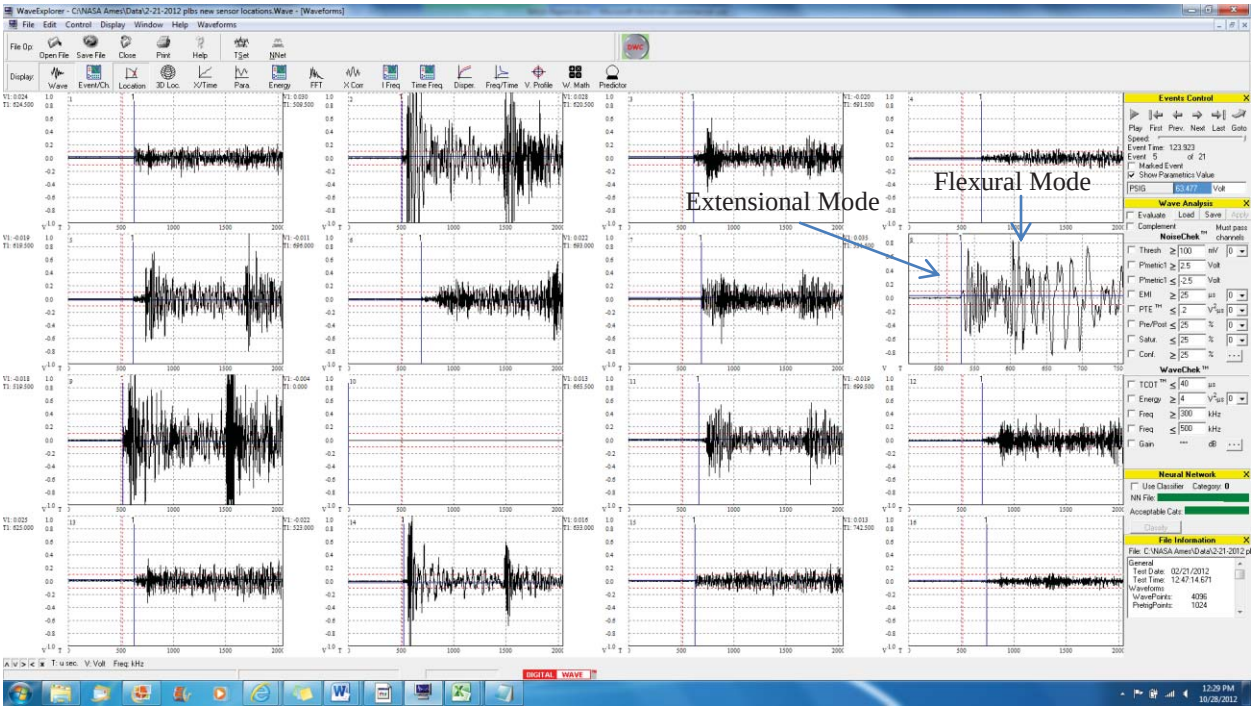

Figure 25 - Captured lead break waveform with extensional mode

The above figure shows a waveform from a lead break at the center notch. The wave modes are labeled. It can be seen that they have the characteristics shown in Figures 18 and 19.

The wave modes have specific frequency-velocity relationships based on the material and thickness of the plate. Figure 26 shows this relationship in the form of a dispersion curve for the A.O. Smith pressure vessel used in this testing (see reference 5) for more information on dispersion curves). It can be seen that at the lower frequencies, the extensional mode propagates at a higher velocity than the flexural mode. That is why the extensional mode arrives first in the waveforms. When performing source location, it is important to know which wave modes are being generated, so that the correct velocity is used in the source location algorithms.

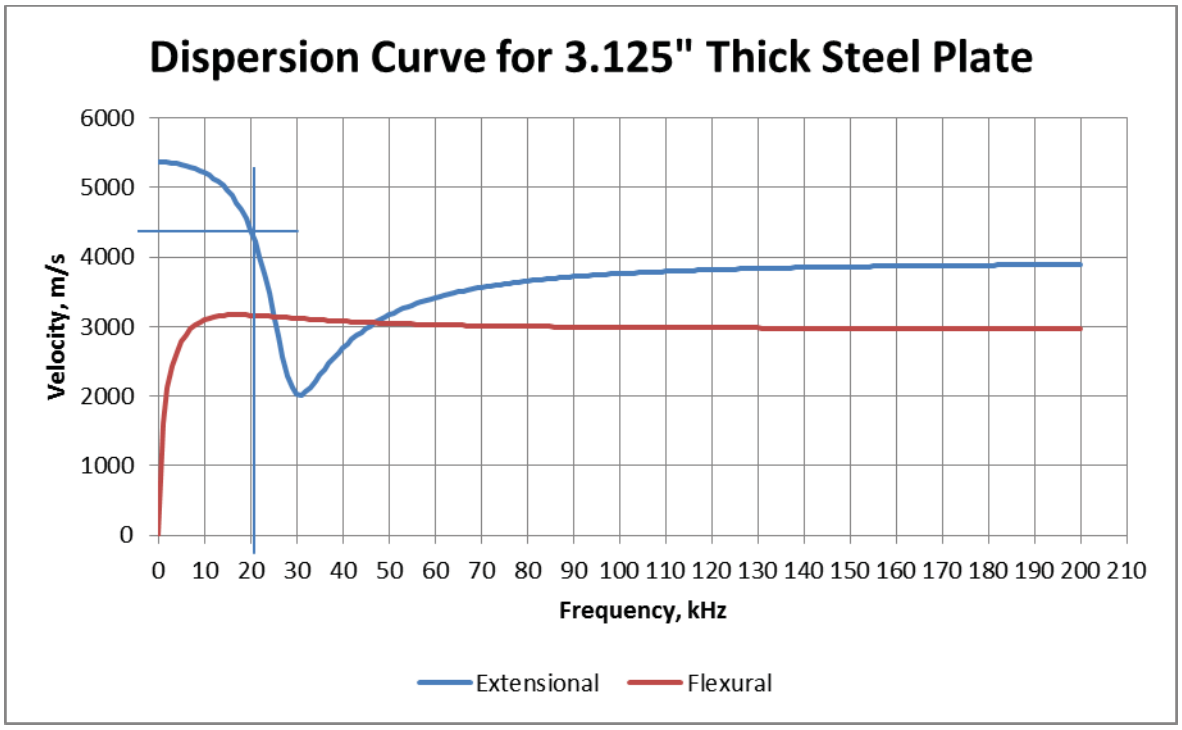

Figure 26 - Extensional and Flexural mode dispersion curves for 3.125 inch thick steel plate

In this figure, the 21 kHz location for the extensional mode is marked. The extensional mode velocity at this point is approximately 4400 m/s. The dispersion curve plot was generated by the WaveExplorer™ software.

PLB Location Accuracy

The accuracy of the 2-D source location algorithms were checked using the lead breaks in the notches. Since the waveforms have good extensional mode formation, the extensional mode velocity was used for the source location. The software calculates the differences in arrival times and from those can determine the location of the source. From Figures 27 and 28 it can be seen that both sensor arrays resulted in source location well within six inches of the lead break location. This provides adequate accuracy for follow up inspections, if needed.

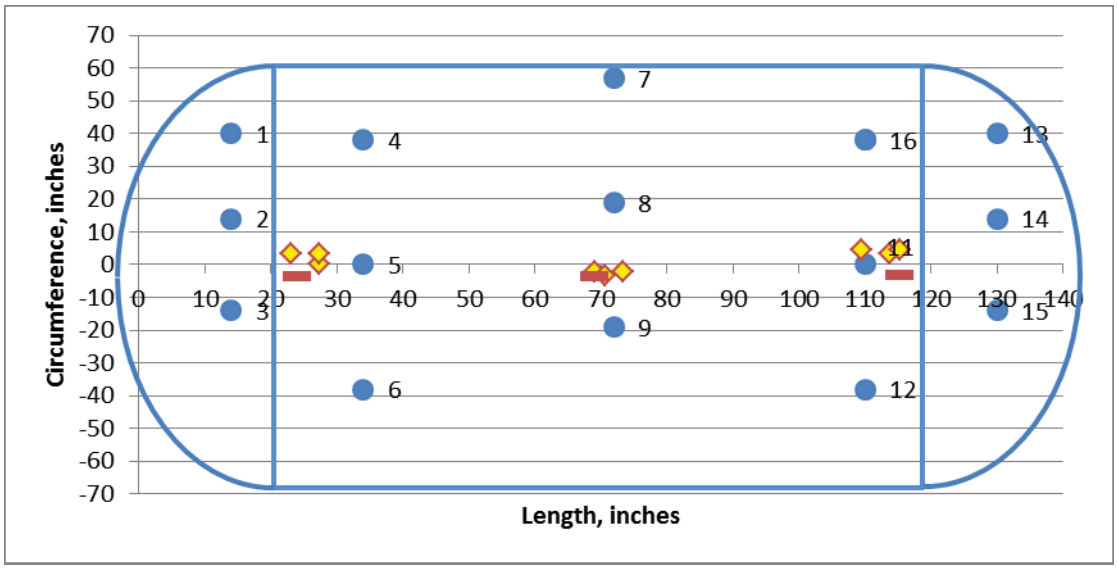

Figure 27 - Lead break source locations on the test vessel with head sensors

Lead break locations as found with the WaveExplorer™ software for lead breaks in the three notches machined into the vessel are shown in the above figure. The blue circles are sensor locations, the red lines are the flaw locations, and the yellow diamonds are the lead break locations.

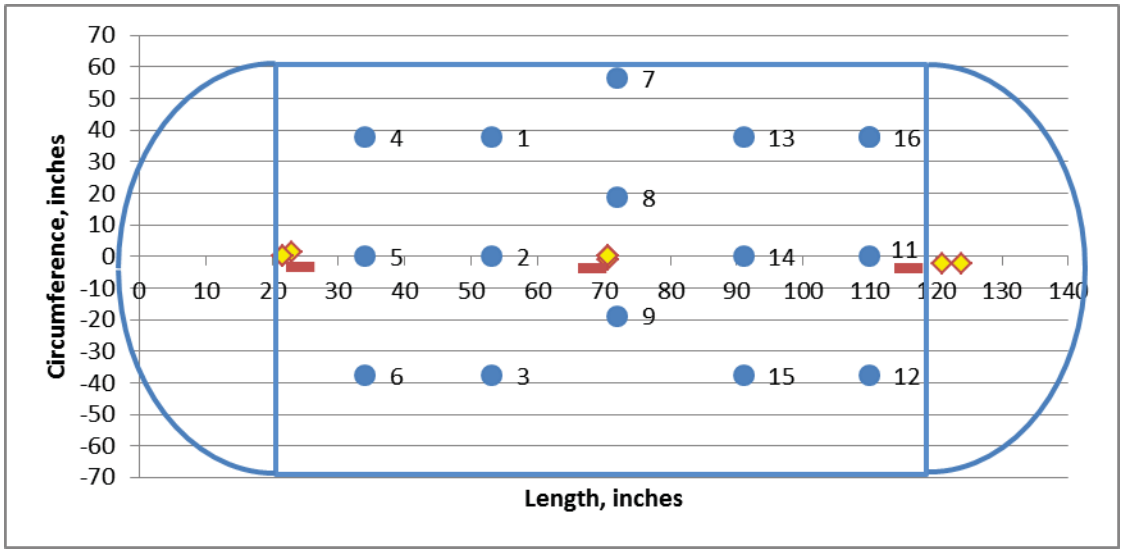

Figure 28 - Lead break source locations on the test vessel without head sensors

Lead break locations as found with the WaveExplorer™ software for lead breaks in the three notches machined into the vessel, without AE sensors located on the heads. The blue circles are sensor locations, the red lines are the flaw locations, and the yellow diamonds are the lead break locations.

Test Results

The table in Appendix A shows the number of cycles and the pressure range over which the cycles were performed. The data files from each test are shown as well. The comments to the right were made during the testing so that any changes in sensor locations or test parameters could be noted.

The vessel and the notches at the welds were remotely monitored using digital video cameras, Figure 29. The center notch had a video microscope mounted above it to monitor the crack at that notch. A pan and zoom video camera was mounted in the test bunker to monitor the pump and test fixtures so that entry into the bunker during pressurizations was not required.

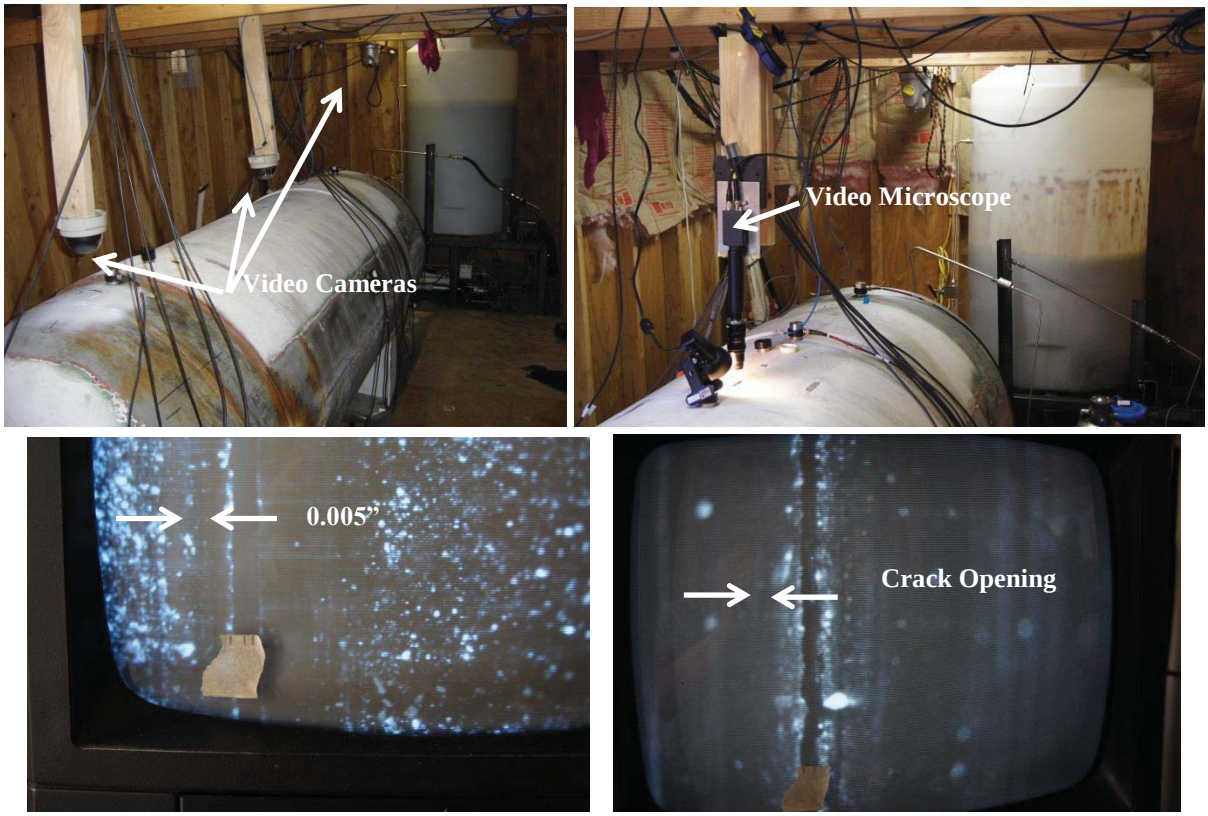

Figure 29 - Vessel with Video Microscope Images

This array of photographs, starting in the upper left corner and proceeding clockwise shows; the vessel with sensors attached (magnetically held in place) and the video cameras monitoring the notches at the welds; the video microscope mounted from the ceiling of the bunker monitoring the crack in the center flaw; a picture of the monitor for the video microscope showing the crack in the center flaw at 14,000 psi; and a picture of a pair of calipers held under the video microscope, opened to 0.005”. From this it can be seen that the crack opened slightly under 0.005” at 14,000 psi.

The WaveExplorer^{TM} system was set to the parameters outlined in Section 3, and the vessel was monitored during the cycles. The acquisition settings on the WaveExplorer^{TM} system were set conservatively. This resulted in large data sets, but since the data was digitized and stored, it was

felt that it was better to acquire extra data and not miss flaw growth events, than to limit the data acquisition and possibly miss crack growth.

Along with the modal AE data, pressure, strain and temperature data were acquired and stored.

After the data was digitized and stored, it was then sorted using algorithms that analyzed the number of channels that crossed the 32 dB_{AE} threshold, saturation of the signals, energy level of the signals, pretrigger noise, and frequency content. A short explanation of each filtering step is given below.

Threshold: This was set so that at least three channels had to cross the threshold. This was required so that the 2-D source location could be performed. This insured that the source of the event was the notches.

Energy: Small amplitude signals will cross the threshold settings, but still not have enough wave mode definition to be accurately identified as noise or flaw growth signals. This setting will eliminate signals that cannot be properly identified via modal content.

Saturation: If the signals are so large that they saturate the analog amplifiers or the A/D, then there is no useful information in these signals. This filter removes these signals from the data set. As a note, fatigue crack growth signals during stable fatigue crack growth are typically small amplitude (see Appendix B), while noise sources, such as mechanical rubbing of saddles, surface corrosion, weld slag, etc., are much larger energy sources. Thus, when the gain is set to the ASTM E1419 standard, noise sources are so large they saturate the system amplifiers.

Pretrigger Noise: If the front end of the signal is not clearly defined, either due to flow noise or mechanical noise, the signal cannot be analyzed for modal characteristics, nor can the location of the source be determined. These signals are removed.

Frequency Content: Flaw growth signals contain higher frequency content, due to the short rise time of the fracture source. Noise signals do not have this characteristic. Signals not meeting the flaw growth signal frequency requirements are removed.

The data files were first analyzed manually until flaw growth data from the center crack location was observed. This data was then used to set the filtering parameters described above. Appendix C contains the filter settings. The results of this filtering resulted in removal of at least 95% of the waveforms, and in many instances almost 99%. This reduced the number of events per file from 50,000 to 100,000 events, to approximately 1000 to 5000 events. The remaining events were then manually reviewed for modal characteristics to determine if they were from flaw growth.

Shown in Figure 30 is a waveform from earlier in the testing that was located at the center notch. Prior experience has shown that heuristically the approximate first arriving frequency in the extensional mode can be estimated using $\lambda=c/f$, where λ the wall thickness multiplied by four (4), c is the extensional mode propagation velocity, and f is the frequency. Assuming a wall thickness of approximately 3 inches (recall that the plate layers are tightly coupled acoustically) and an extensional mode velocity of 185,000 in/s (as measured from lead breaks), results in a frequency of 15.4 kHz. It should be noted that this is a quick "rule-of-thumb" approach, based

on data from wave propagation measurements in varying thicknesses of steel and aluminum plates and then manually measuring the frequency of the first cycle of the extensional mode, and then applying a "fit" to the data, not waveform theory (see dispersion curve discussion in Section 6, Wave mode formation). Variations could occur based on the frequency content of the source, or the source orientation. With this said, comparing this 15.4 kHz estimated frequency to the measured frequency of 21 kHz (see Fig. 30 below, which correlates exactly with the dispersion curve calculation shown in Fig. 26), shows the usefulness of the simplified method, and proves that the wave was propagating through the entire wall of the vessel, not just in the outer layer. If the wave were propagating only in the outer layer, the frequency of the extensional mode would have been much higher. As a final note, plate waves can take anywhere from 30 to 100 plate thicknesses to fully form *(reference 4, Weaver & Pao)*, which for this vessel would be 90 to 300 inches from the source, although wave attenuation effects at the longer distances make detection problematic, particularly low energy signals in multilayer and thick single vessels. Sensor 15 was approximately 60 inches from the source, so full mode formation may not have occurred, thus the frequency may not be entirely representative. There were few of these events observed in the data, and the reasons for this are discussed later in the paper.

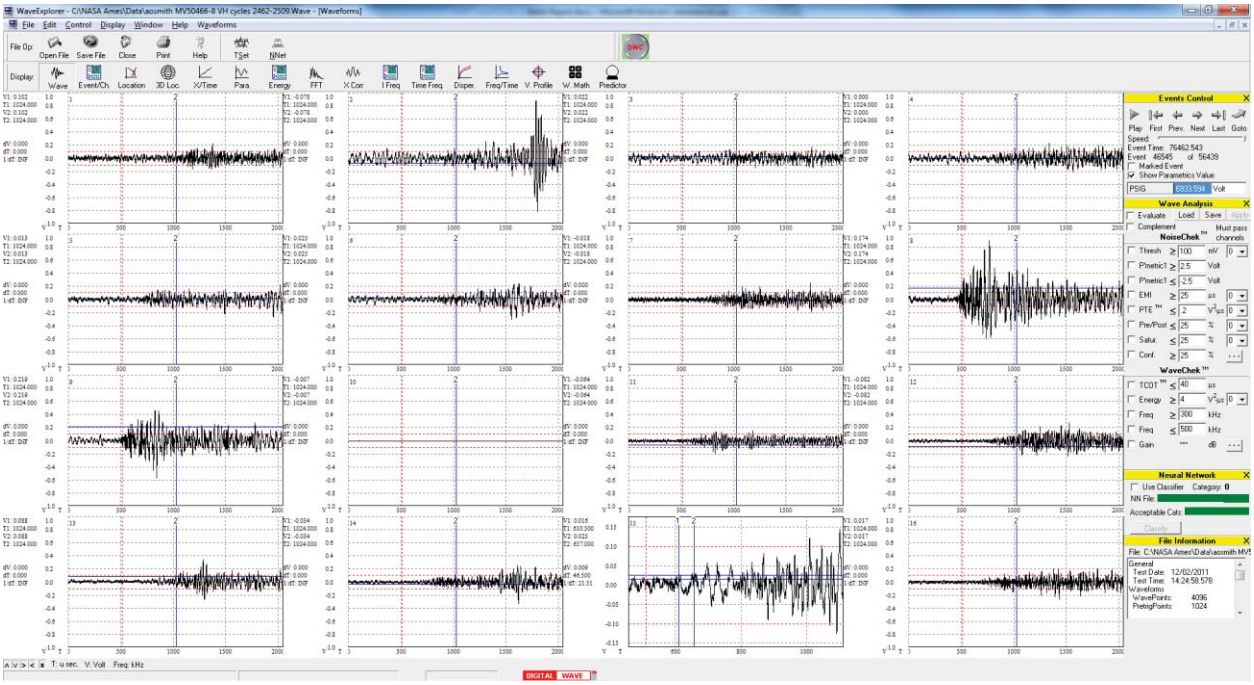

Figure 30 - Crack growth event plots, cycles 2462-2509

For the events shown above, the simultaneous arrival at sensors 8 and 9 are the quick indicators of the location. This event occurred at a pressure of 6933 psi, near the peak pressure of the cycle, 7260 psi. Channel 15 has been expanded to show the front end frequency of the waveform. This was measured at 21 kHz.

Other events with source locations at the center notch were also seen in the data, with front end frequencies of the waveforms in the range of 30-40 kHz, slightly higher than the expected frequency of 15.4 kHz for this thickness of vessel. These may be examples of how the source

function (crack growth) may not contain the sufficient frequency content due to non-brittle fracture, as discussed later.

These waveforms were also useful in that they showed that the frequency content of the crack growth signals resulted in greater frequency content over 200 kHz, than just noise signals, Figure 31. This information was used to filter the data by looking at the percentage of energy in the signals over 200 kHz, and eliminating signals that did not have enough content in this frequency range. See Figure 32 for a typical noise signal Fast Fourier Transform (FFT).

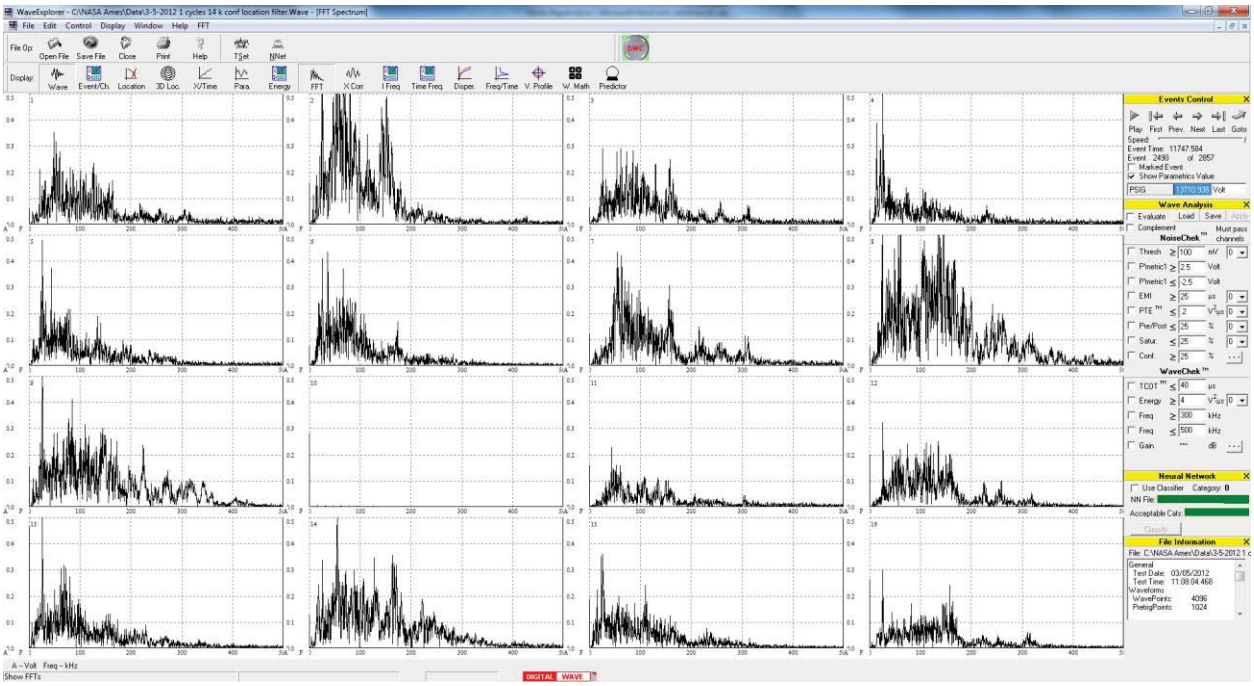

Figure 31 - FFT of crack growth signal

Note the frequencies above 200 kHz in channels 8 and 9. This frequency is an indicator of possible crack growth.

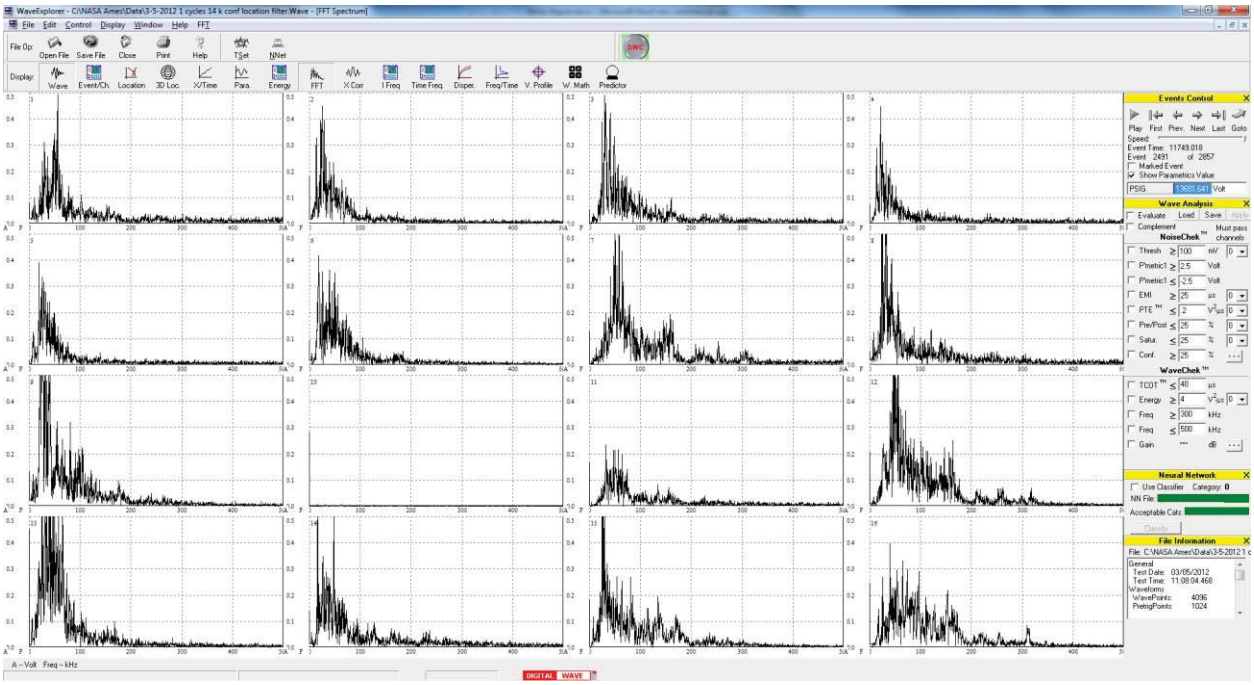

Figure 32 - Typical FFT of noise.

Note the lack of higher frequency content in the noise signal.

The final portion of the testing (completion was forced due to budget limitations) was an over-pressure of the vessel to 14,000 psi, which was intended to put the outer layer near nominal yield stress to force crack growth since it was uncertain at the time how deep the visible crack was. The working pressure of the vessel was 6600 psi, with a factor of safety of 2 on nominal yield stress. By pressuring to 14,000 psi, the vessel was pressurized to 2.12 times working pressure, 6% over its factor of safety design pressure. Many safety precautions were taken throughout this testing, and four of these cycles were completed without incident before the last remaining hydraulic pump failed and the test was terminated after consultation with NASA.

It was also determined that pressurizing to this level did put the vessel outer wall into some plastic deformation (see Figures 14, 15 and 16 showing the Pressure-Strain curves), and thus plastically deformed the notch. This was done in order to see if a large enough energy release could be obtained for crack growth detection. During this pressurization, there were several small events from the notch that were detected. However, there was one larger energy event, with mode formation, that was captured, and is shown in Figure 33 (an expanded view of channel 8 is shown in Figure 34 showing the wave mode details). This particular event, while emanating from the notch, did not meet the extensional mode front end frequency calculation described earlier, of 15.4 kHz. In hindsight, this is not unexpected since the source for this waveform would definitely not have been brittle fracture. Thus, most likely the source did not contain the low frequency components that would form the front end of the extension mode.

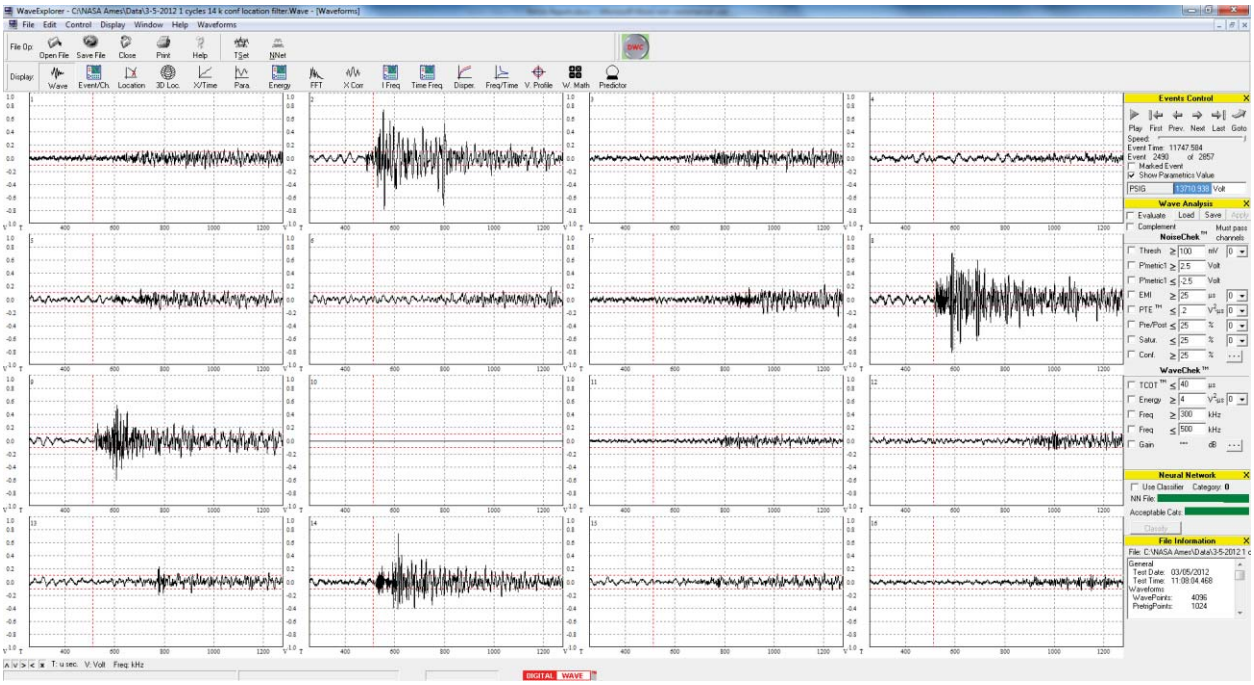

Figure 33 - Crack growth signal at 13.710 psi

The crack growth signal during over-pressurization shown above occurred at a pressure of 13,710 psi. Note the nearly simultaneous arrival times at sensors 2, 8, 9 and 14. This would be observed for flaw growth from the center notch, for the sensor arrangement in Figure 28.

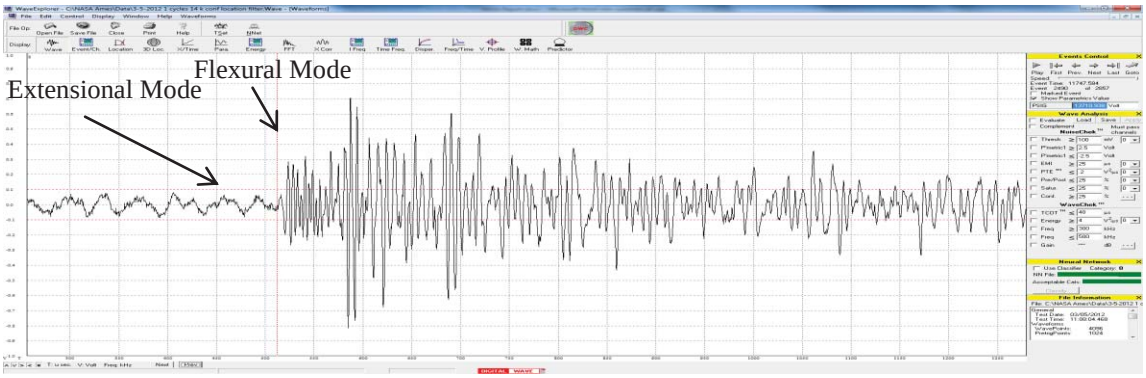

Figure 34 - Expanded view of Channel 8 showing the extensional mode formation

The trailing wake in the event shown above is due to waves propagating around the vessel. The x-axis divisions are 100 μseconds.

Section 7. Discussion of Test Results

In the testing of the vessel, the crack growth did not result in brittle fracture of the fatigue crack. This is discussed in the following section.

In determining the depth of the notch, the main driver was the amount of time available for the testing. The original time frame for the fatigue testing was a three month period. The Haskel pump that was used for the pressurization took approximately 45-60 minutes for each cycle. That meant approximately 30 cycles per day, accounting for maintenance and repair down time. Based on these constraints, it was decided to machine the notches in the outer

wrap to a depth of 0.175 inches, which from the facture mechanics should result in approximately 0.055 inches of crack growth over the three month period, Figure 24. It was felt that this was a reasonable amount of crack growth over this shortened time frame to capture fatigue crack growth data, without the crack going through-wall. However, the MAE data from the cyclic fatigue testing was not as definitive as hoped. Except for a few events, the wave propagation characteristics were not well defined. After review of the notch geometry, it may have been machined too deep in an attempt to insure that the crack grew in the first few hundred cycles. At the 0.175 inch depth, the stress at the notch would have been in the range of 100 ksi. This would have been beyond the elastic limit of the steel, per NASA TM X-3316 [Ref. 11] measurements. Fracture of the notch would have not been brittle fracture (plane strain), but plastic fracture. Brittle fracture releases the energy in a much shorter time frame, creating the frequency content needed for clear mode formation. This can be thought of as the difference between a dry twig and a green twig fracturing. The dry twig snaps with a sharp, loud sound and a clean break. The green twig bends, deforms, and then fails over multiple surfaces, with little sound. If the fatigue fracture was elastic-plastic in the vessel, then the energy release was either out-of-plane or too slow, resulting in poor mode formation and energy release below the theoretical calculated sensitivity as shown in Appendix B, which assumes brittle fracture.

A photograph of the crack surface that was obtained by Southwest Research Institute on subcontract as reported in Ref. 7 is shown in Figure 35. The various facture surfaces are shown in the photograph.

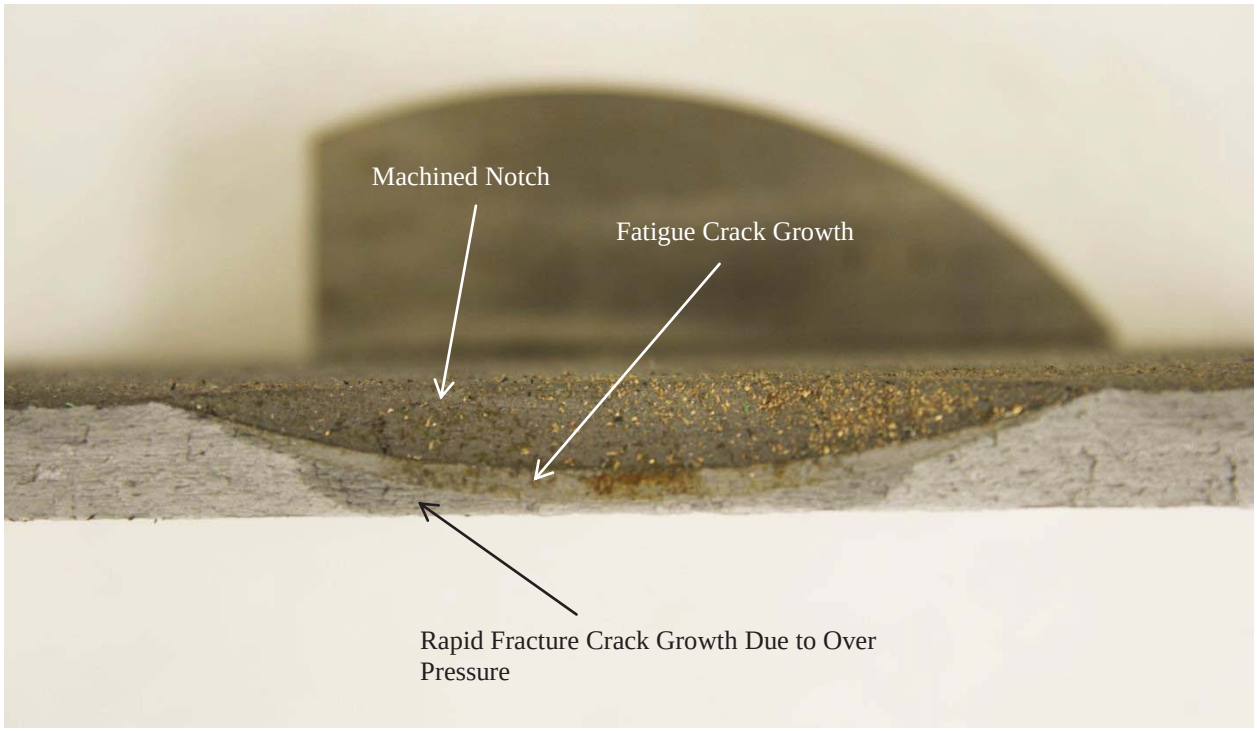

Figure 35 - Photograph of One Face of the As-Opened Crack (credit SwRI, Ref 7)

The photograph shows the cross section of the notch after the layer was fractured open. The dark gray area is the machined notch, the lighter gray area underneath the notch is the fatigue crack, the darker area under that is the rapid fracture area due to the overload near the end of the test (Ref 7, Southwest Research Institute).

The elastic-plastic analysis is supported by the follow-on fracture mechanics and SEM images of the fracture surface (Ref. 7, SwRI). The photographs show both transgranular and a significant amount of intergranular fracture surfaces, along with secondary (out of plane) cracking and dimpled cup and cone associated with ductile fracture. Since transgranular failure is associated with brittle fracture, while intergranular is normally associated with ductile (overload) failure (Janssen, et. al., *Fracture Mechanics*, Ref. 8), it is concluded that the loading for the vessel at the notch was in the elastic-plastic regime, which was borne out by their assessment that the actual stress intensity factor at the crack (K1) during these cycles was 85.6 ksi√inch, nearly equal to the average plane stress fracture toughness (Kc) of 90 ksi√inch obtained in their material testing (and which was revised upward to 170 ksi√inch in their Phase 2 report, Ref [9] . This likely lead to the sensitivity and mode formation loss observed in the waveform data due to the out-of-plane tearing of the material, as opposed to the transgranular in-plane brittle fracturing.

Prior DOT and ASME Pressure Vessel Testing

Digital Wave Corporation has performed fatigue crack growth testing on high strength steels used for DOT and ASME specification pressure vessels that operate at high (1800-5000 psi) pressures. This testing has shown that shown that brittle fatigue results in waveforms with definite modes in these monolithic (non-layered) vessels.
A comparison of the data from the A.O. Smith pressure vessel to the data captured during the testing phase to develop an ASME Code Case (Case 2390-5, Composite Reinforced Pressure Vessels, Section VIII, Division 3, now incorporated in KF-1216 and KE-5 of Sect. VIII, Div. 3) will be shown in this section. This Code Case is for the use of acoustic emission for the certification of the laminate, but the steel liner was also monitored during the test. The vessels for this Code Case were Type 2 construction vessels, with a one inch thick steel liner and a one inch thick fiberglass composite overwrap, with exposed domes. During the cyclic testing of the vessels, sensors were mounted on the exposed steel domes to determine if modal acoustic emission could detect fatigue cracking in the long seam weld of the steel liner. Channels 1-4 where on one dome, channels 5-8 were on the opposite dome. The vessel was 20 feet long. In one of the test vessels, an interior shelf, or lip, occurred in the weld, and fatigue cracking began to occur at this location. Modal AE was able to discriminate between the cracking occurring in the composite from that in the weld. Figure 36 shows a crack growth signals from the long seam weld. The same gain settings were used for this testing as for the A. O. Smith pressure vessel. The crack growth signals captured from the fatigue crack growth in these vessels were similar in energy to the signals captured during the A. O. Smith pressure vessels tests.

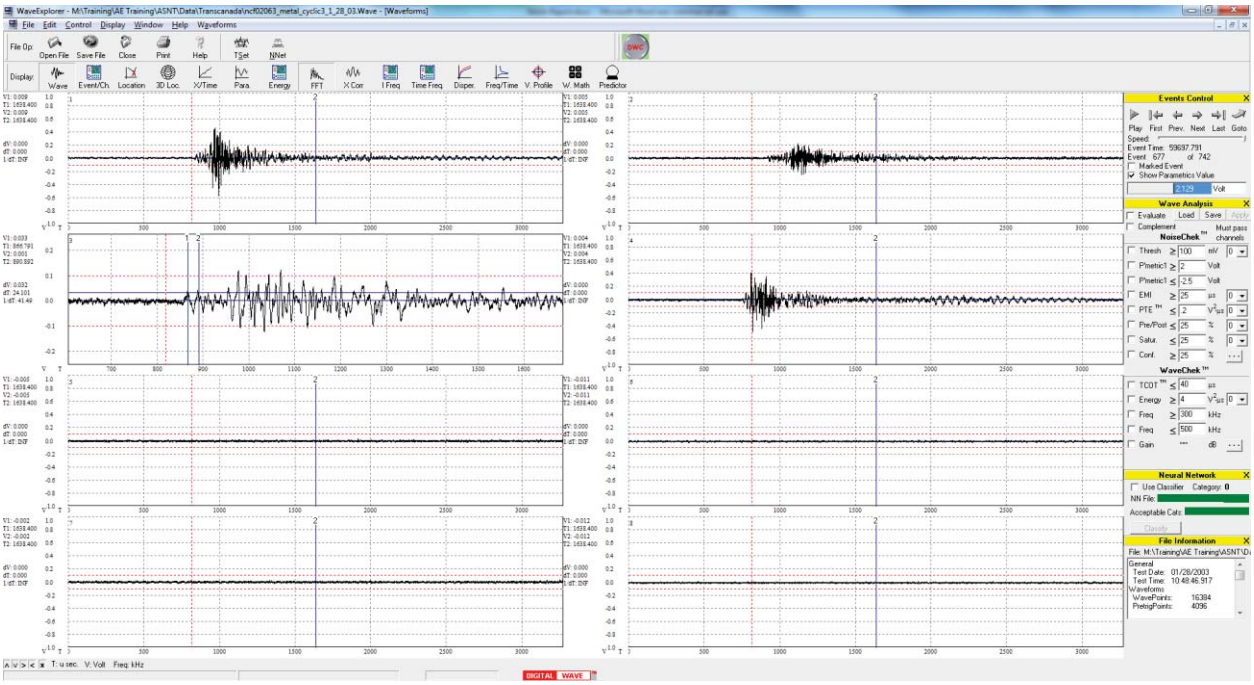

Figure 36 - MAE monitoring of a Type 2 COPV with 1 inch liner vessel

The above figure shows fatigue crack growth waveforms from a long seam weld in a type 2 vessel. Channel 3 has been expanded to show the mode formation.

The frequency content of the signals is shown in Figure 37. From this it can be seen that the crack growth signals from this vessel contain frequencies above 200 kHz, just like those from the A. O. Smith pressure vessel. Thus, this discriminator, along with extensional mode formation, can be used to filter data in high strength steel pressure vessels.

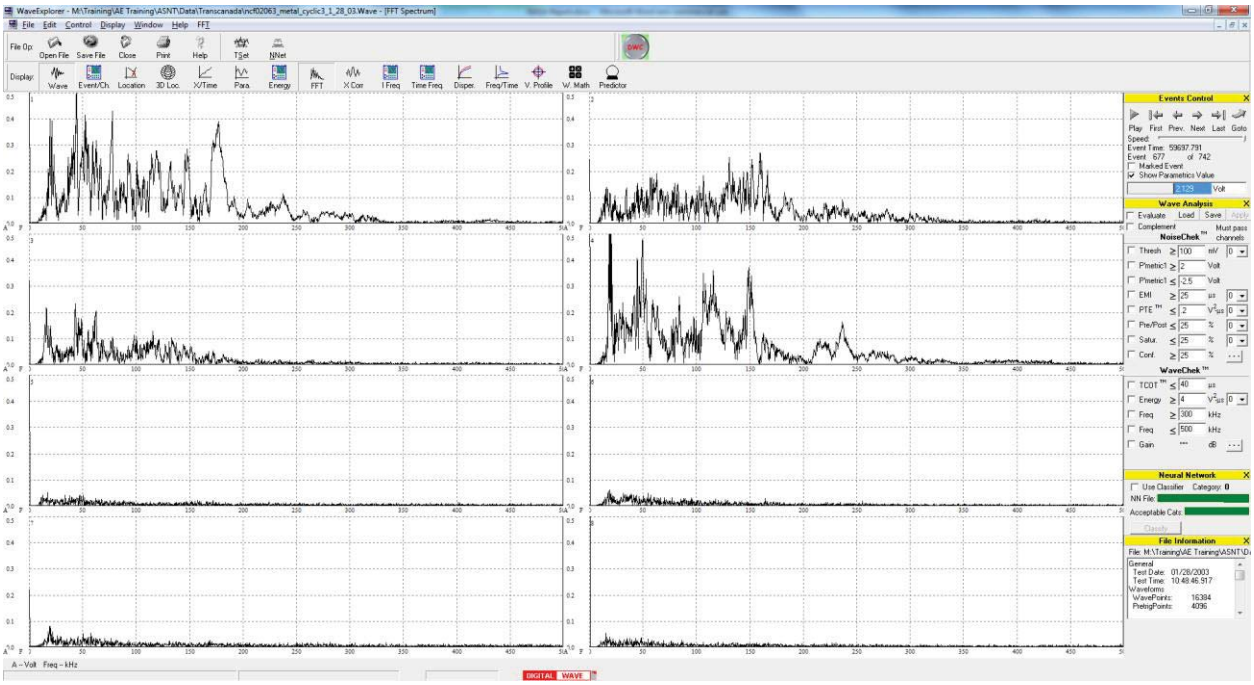

Figure 37 - FFT of the signals in Figure 36

This figure shows the FFT (frequency content) of the signals in Figure 36. The x axis is frequency, in kHz, and the y axis is amplitude. The main feature to note is the signal content over 200 kHz. This corresponds closely with the data from the fatigue testing of the A. O. Smith pressure vessel.

Section 8. Conclusions

The following are the principal conclusions from the MAE cyclic crack growth testing.

1. Crack growth was detected – Crack growth signals were captured from the center notch, and identified via frequency content and source location. There were not many detectable events, which was likely due to elastic-plastic fracture of the steel. Due to time and budget limitations, and the amount of data captured during the testing, crack growth data from the other notches were not analyzed.
2. Wave Modes – Extensional mode formation was observed in some of the events, but not in others. This was likely an indication that the failure mode of the vessel was not brittle fracture, but elastic-plastic fracture. This would change the expected frequency content of the signal, as well as the mode shape, since the source would not be in-plane with the large extensional modes.
3. Frequency content can be used as discriminator/filter – One of the main results to come out of this test is the frequency content of the crack signals. Crack signals showed higher frequency content above 200 kHz. This aided greatly in removing noise signals from the data, reducing data by 95-99%. This reduction then allows manual discrimination of the remaining data based on wave mode formation.
4. Data matches that from other pressure vessel fatigue tests – The crack growth data was similar to that from fatigue tests on DOT ad ASME high strength pressure vessels.

5. Crack growth was elastic-plastic – The SEM photographs of the fracture surfaces provided by SwRI in Ref. 7 clearly showed the failure of the steel was in the elastic-plastic zone (e.g., intermittent and even infrequent striations, and clear physical indications of plastic tearing), and thus the expected brittle fracture behavior of the vessel (due to its relatively high tensile strength below ambient test temperatures) was not achieved during this testing.
6. Data Analysis – From this testing, the difficulties in sorting crack growth signals from noise are clearly evident. Due to the construction of the vessels, noise sources are abundant and varied. The ability to detect these sources requires detailed knowledge of the fracture mechanics and the resulting wave propagation due to the fracture of the material. Simple analysis routines based on gross waveform parameters cannot be used to analyze these complex waveforms. Extensive post-test analysis by the investigator showed that filters could be useful in further refinement of data for identification of a relevant source, but this would likely need to be validated in further testing to gain general acceptance.
7. Correlation with physical results – The SwRI data [Ref 7]shows that crack grew downward, through the thickness, but not lengthwise, and that the average depth extensions (da's) per cycle (dN's) were in the range of 7.2E-6 (early growth) to 1.8E-5 inches per cycle near the end of the test. Cumulatively, about 0.064 inches of growth was achieved with the pressure cycling prior to the rapid growth with the yield stress level cycles at the end.
8. It was widely expected by all involved that this would be an easy crack to locate and characterize with the MAE method, but for the reasons discussed, it proved to be possible, but very difficult.

Section 9. Follow-on Testing

The following are logical objectives for future testing, if possible.

1. Review of data from the other notches - existing data from the other notches (near each head) have not been reviewed due to funding and schedule constraints. A first step would be to analyze the data from these stress risers.
2. Stress analysis of head-to-shell weld - The most likely point of failure for these vessels based on industry experience is the failure of the head-to-shell weld, and then the head blowing off during pressurization, or nozzle failures. Notches were not machined in the head-to-shell welds or nozzles because the stress was unknown in this region (due to unknown weld residual stresses) and because the lower level of cyclic stress in the longitudinal direction would likely have required many more cycles to grow a crack significantly, and there was insufficient funding to support that amount of cycling. Because of this, it was not felt that a reasonable machined notch depth could be determined, and this could lead to either catastrophic failure or no crack growth at all. Either result was not acceptable for the test objectives. Thus, a thorough stress analysis would be very useful for determining the required parameters of a machined circumferential flaw that would be safe and achieve growth in a reasonable number of cycles. This approach will need to incorporate any weld geometry variations observed in these vessels, as well as welding variabilities.

3. Determine notch depth and shape for circumferential notch in head-to-shell weld at heat affected zone (HAZ) – Once the stress analysis is performed, then a notch depth that would still result in a 5-10 year life at the cyclic intervals of pressurization could be machined into the HAZ at the head-to-shell weld. This would result in crack growth more typical of the failures expected in the A. O. Smith pressure vessels. Then perform additional cyclic fatigue testing and MAE – Repeat the test program, but with the head-to-shell weld notches. Such notches are more representative of flaws that what would likely exist in these vessels, and they would be in thick material with a much lower applied delta stress intensity factor. Consequently, their crack growth would be in the brittle crack growth regime, with extensional wave formation that would be more readily detectable by the MAE method.
4. Determine notch size for elastic fracture in parent material in outer wrap – If failure in the parent material in the outer wrap is of interest (since individual layer failure can be tolerated, and inner layer cracking can be detected with leak monitoring, this question should be considered), then a smaller EDM notch depth for earlier-life elastic fracture should be calculated and machined in the vessel so that a more likely, realistic correct crack growth acoustic signal is developed. Include this notch in the repeat test described above.
5. Perform laboratory testing on samples from wrap layers from A. O. Smith vessel – Fatigue test specimens from vessel MV50466-8 could be machined and fatigue tested in the lab using a servo-hydraulic test machine. These specimens could be instrumented with MAE sensors, and crack growth monitored during rapid cycling to determine fatigue crack growth energies with direct correlation to captured MAE waveforms and FFT assessments.

Section 10. References

1 Blackburn, P.R., Rana, M.D., "Acoustic Emission Testing and Structural Evaluation of Seamless, Steel Tubes in Compressed Gas Service," *Journal of Pressure Vessel Technology*, May 1986, vol. 108, pp. 234-240.

2 Gorman, M.R., "Plate Wave Acoustic Emission," *Journal of the Acoustical Society of America*, 1991, vol. 90, no. 1, pp. 358-365.

3 Gorman, M.R., Prosser, W.H., "AE Source Orientation by Plate Wave Analysis," *Journal of Acoustic Emission*, 1991, vol. 9, no. 4, 283-288.

4 Weaver, R. L., Pao, Y.H., *Axisymmetric Elastic Waves Excited by a Point Source in Plate*, **Journal of Applied Mechanics**, December, 1982, Vol. 49, pp. 821-836

5 Graff, K. F., "Wave Motion in Elastic Solids," Dover Publications, 1975.

6 Barsom, J.M., Rolfe, S. T., "Fracture and Fatigue Control in Structures, Applications of Fracture Mechanics," Second Edition, Prentice-Hall, 1987, p. 48

7 Cardinal, J.W., Popelar, C. F., and Page, R.A., Revised Final Report, Southwest Research Institute (SwRI) Project No. 17408 *"Multilayer Pressure Vessel Materials Testing and Analysis (Phase I)", Cardinal, Joseph W, Revision 1, November 6, 2012*

8 Janssen, Zuidema, Wanhill, *Fracture Mechanics*, VSSD, Second Edition, 2002-2006, pp. 286, 294-295

9 Cardinal, J.W. and Popelar, C. F., Multilayer Pressure Vessel Materials Testing and Analysis (Phase 2), Southwest Research Institute, SwRI® Project No. 18.17633, Final Report (Rev 01), September 2013

10 Hudak, Connolly, Hanley & Lukezich, A Damage Tolerance Approach for Recertification of Submarine High-Pressure Flasks, SwRI Project No. 06-4557, Department of the Air Force, Sacramento Air Logistics Center, Contractual Engineering Task #TIE-91-335, Southwest Research Institute, March 31, 1995

11 Hudson, M.C., Newman, J.C., & Lewis, P.E., An Investigation of Fracture Toughness, Fatigue-crack Growth, Sustained Load Flaw Growth, and Impact Properties of Three Pressure Vessel Steels, NASA Technical Memorandum X-3315, Langley Research Center, December, 1975

12 DOT SP-15322 – Digital Wave Corp, Use of Modal Acoustic Emission and ultrasonic examination (AE/UE) in lieu of hydrostatic pressure test and internal visual examination, April 26, 2012.

13 Ziola, S. M., AE Qualification Test of HPADS Storage Vessel #16 at N250A, Ames Research Center, Moffett Field, CA, Digital Wave Corp., 10/10/2001

14 Ziola, S. M., AE Qualification Test of HPADS Storage Vessels 21 - 36 at N250A, Ames Research Center, Moffett Field, CA, Digital Wave Corp., 10/29/2002

15 Ziola, S. M., AE Qualification Test of HPADS Storage Vessels 1 - 16 at N250A, Ames Research Center, Moffett Field, CA, Digital Wave Corp., 8/12/2009

16 ASTM E-1419 – 02b – Standard Test Method for Examination of Seamless, Gas Filled Pressure Vessels using Acoustic Emission

Appendix A. Table of Test Files

Total Number of Cycles	Date	Cycles per File	Filename	Notes
10	9/23/11	10	aosmith MV50466-8 VH cycles 1-10.Wave	3000-6600 psi
15	9/26/11	5	aosmith MV50466-8 VH cycles 11-15.Wave	3000-6600 psi
19	9/26/11	4	aosmith MV50466-8 VH cycles 16-19.Wave	3000-6600 psi
29	9/26/11	10	aosmith MV50466-8 VH cycles 20-29.Wave	3000-6600 psi
31	9/26/11	2	aosmith MV50466-8 VH cycles 30.Wave	3000-6600 psi
40	9/27/11	9	aosmith MV50466-8 VH cycles 31-40.Wave	3000-6600 psi
45	9/27/11	5	aosmith MV50466-8 VH cycles 41-45.Wave	3000-6600 psi
65	9/27/11	20	aosmith MV50466-8 VH cycles 46-65.Wave	3000-6600 psi
95	9/28/11	30	aosmith MV50466-8 VH cycles 66-95.Wave	3000-6600 psi, lead breaks at each notch
114	9/29/11	19	aosmith MV50466-8 VH cycles 96-114.Wave	3000-6600 psi
131	9/29/11	17	aosmith MV50466-8 VH cycles 115-131.Wave	3000-6600 psi
144	9/30/11	13	aosmith MV50466-8 VH cycles 132-144.Wave	3000-6600 psi
146	9/30/11	2	aosmith MV50466-8 VH cycles 145-146.Wave	3000-6600 psi
157	9/30/11	11	aosmith MV50466-8 VH cycles 147-157.Wave	3000-6600 psi
196	10/3/11	39	aosmith MV50466-8 VH cycles 158-196.Wave	3000-6600 psi, 3 cycles ran before AE started recording
200	10/4/11	4	aosmith MV50466-8 VH cycles 197-200.Wave	3000-6600 psi, gauge leaking
202	10/4/11	2	aosmith MV50466-8 VH cycles 201-202.Wave	3000-6600 psi, changed sensor 3
219	10/5/11	17	aosmith MV50466-8 VH cycles 203-219.Wave	2500-6600 psi
245	10/6/11	26	aosmith MV50466-8 VH cycles 220-245.Wave	2500-6600 psi, one 7000 pressurization cycle
256	10/6/11	11	aosmith MV50466-8 VH cycles 246-256.Wave	2500-6600 psi, one 7300 pressurization cycle
257	10/6/11	1	aosmith MV50466-8 VH cycles 257-257.Wave	3000-6500 psi
270	10/7/11	13	aosmith MV50466-8 VH cycles 258-270.Wave	2500-6600 psi
271	10/8/11	1	aosmith MV50466-8 VH cycles 258-270.Wave	2500-6600 psi
272	10/8/11	1	aosmith MV50466-8 VH cycles 271-271.Wave	2500-6600 psi, Strain gages lost
276	10/10/11	4	aosmith MV50466-8 VH cycles 272-275.Wave	2500-6600 psi
305	10/11/11	29	aosmith MV50466-8 VH cycles 276-305.Wave	500-6600 psi
330	10/12/11	25	aosmith MV50466-8 VH cycles 306-330.Wave	500-6600 psi
358	10/12/11	28	aosmith MV50466-8 VH cycles 331-358.Wave	500-6600 psi
390	10/13/11	32	aosmith MV50466-8 VH cycles 359-390.Wave	500-6600 psi
413	10/13/11	23	aosmith MV50466-8 VH cycles 391-413.Wave	500-6600 psi
446	10/14/11	33	aosmith MV50466-8 VH cycles 414-446.Wave	500-6600 psi
449	10/14/11	3	aosmith MV50466-8 VH cycles 447-449.Wave	500-6600 psi
542	10/16/11	93	aosmith MV50466-8 VH cycles 450-542.Wave	1000-6600 psi
580	10/17/11	38	aosmith MV50466-8 VH cycles 543-580.Wave	1000-6600 psi
602	10/17/11	22	aosmith MV50466-8 VH cycles 581-602.Wave	1000-6600 psi
634	10/18/11	32	aosmith MV50466-8 VH cycles 603-634.Wave	1000-6600 psi
646	10/18/11	12	aosmith MV50466-8 VH cycles 635-646.Wave	1000-6600 psi, Strain gages back on - all 0.25" rosettes
691	10/19/11	45	aosmith MV50466-8 VH cycles 647-690.Wave	1000-6600 psi
754	10/20/11	63	aosmith MV50466-8 VH cycles 691-754.Wave	1000-6600 psi

804	10/21/11	50	aosmith MV50466-8 VH cycles 755-804.Wave	1000-6600 psi
844	10/22/11	40	aosmith MV50466-8 VH cycles 805-844.Wave	1000-6600 psi
869	10/23/11	25	aosmith MV50466-8 VH cycles 845-868.Wave	1000-6600 psi
914	10/24/11	45	aosmith MV50466-8 VH cycles 869-913.Wave	1000-6600 psi, check 27048, cycle 42 PTE turned off
959	10/25/11	45	aosmith MV50466-8 VH cycles 914-958.Wave	1000-6600 psi
1002	10/26/11	43	aosmith MV50466-8 VH cycles 959-1001.Wave	1000-6600 psi
1047	10/27/201	45	aosmith MV50466-8 VH cycles 1002-1046.Wave	1000-6600 psi
1097	10/28/11	50	aosmith MV50466-8 VH cycles 1047 - 1097.Wave	1000-6600 psi
1157	10/29/11	60	aosmith MV50466-8 VH cycles 1098-1157.Wave	1000-6600 psi, scribed righthand side of notch, cycles 40-41, time 65,750 sec.
1207	10/30/11	50	aosmith MV50466-8 VH cycles 1158-1207.Wave	1000-6600 psi
1245	10/31/11	38	aosmith MV50466-8 VH cycles 1208 - 1245.Wave	1000-6600 psi, Scribed all notches
1293	11/1/11	48	aosmith MV50466-8 VH cycles 1246-1293.Wave	1000-6600 psi
1341	11/2/11	48	aosmith MV50466-8 VH cycles 1294-1341.Wave	1000-6600 psi
1388	11/3/11	47	aosmith MV50466-8 VH cycles 1342-1388.Wave	1000-6600 psi
1437	11/4/11	49	aosmith MV50466-8 VH cycles 1389-1437.Wave	1000-6600 psi
1496	11/5/11	59	aosmith MV50466-8 VH cycles 1438-1495.Wave	1000-6600 psi
1529	11/6/11	33	aosmith MV50466-8 VH cycles 1496-1528.Wave	1000-6600 psi
1583	11/7/11	54	aosmith MV50466-8 VH cycles 1529-1583.Wave	1000-6600 psi
1631	11/8/11	48	aosmith MV50466-8 VH cycles 1584-1631.Wave	1000-6600 psi
1680	11/9/11	49	aosmith MV50466-8 VH cycles 1632-1680.Wave	1000-6600 psi, lead breaks in notches
1728	11/10/11	48	aosmith MV50466-8 VH cycles 1681-1728.Wave	1000-6600 psi, lead breaks in notches
1776	11/11/11	48	aosmith MV50466-8 VH cycles 1729-1776.Wave	1000-6600 psi
1797	11/12/11	21	aosmith MV50466-8 VH cycles 1777-1797.Wave	1000-6600 psi
1833	11/13/11	36	aosmith MV50466-8 VH cycles 1798-1832.Wave	1000-6600 psi
1881	11/14/11	48	aosmith MV50466-8 VH cycles 1833-1880.Wave	1000-6600 psi
1929	11/15/11	48	aosmith MV50466-8 VH cycles 1881-1929.Wave	1000-6600 psi
1978	11/16/11	49	aosmith MV50466-8 VH cycles 1930-1978.Wave	1000-6600 psi
2027	11/17/11	49	aosmith MV50466-8 VH cycles 1979-2027.Wave	1000-6600 psi
2074	11/18/11	47	aosmith MV50466-8 VH cycles 2028-2074.Wave	1000-6600 psi, run waveutility
2140	11/20/11	66	aosmith MV50466-8 VH cycles 2075-2140.Wave	1000-6600 psi, notches polished
2192	11/21/11	52	aosmith MV50466-8 VH cycles 2141-2192.Wave	1000-6600 pis
2240	11/22/11	48	aosmith MV50466-8 VH cycles 2193-2240.Wave	1000-6600 pis
2279	11/23/11	39	aosmith MV50466-8 VH cycles 2241-2279.Wave	1000-6600 pis
2329	11/29/11	50	aosmith MV50466-8 VH cycles 2280-2328.Wave	1000-6600 pis
2368	11/30/11	39	aosmith MV50466-8 VH cycles 2329-2367.Wave	1000-6600 psi, replaced release valve, flow adjusted
2371	11/30/11	3	aosmith MV50466-8 VH cycles 2368-2370.Wave	pressurized to 7260, PTE filter off over 6200 psi
2418	12/1/11	47	aosmith MV50466-8 VH cycles 2371-2418.Wave	1000-7260 psi
2461	12/2/11	43	aosmith MV50466-8 VH cycles 2419-2461.Wave	1000-7260 psi
2510	12/3/11	49	aosmith MV50466-8 VH cycles 2462-2509.Wave	1000-7260 psi
2547	12/4/11	37	aosmith MV50466-8 VH cycles 2510-2546.Wave	computer locked up, need file fixed
2594	12/5/11	47	aosmith MV50466-8 VH cycles 2547-2594.Wave	1000-7260 psi
2642	12/6/11	48	aosmith MV50466-8 VH cycles 2595-2642.Wave	1000-7260 psi
2687	12/7/11	45	aosmith MV50466-8 VH cycles 2643-2687.Wave	1000-7260 psi
2734	12/8/11	47	aosmith MV50466-8 VH cycles 2688-2734.Wave	**hard disk full, WE locked up, no idea for number of cycles**

2771	12/9/11	37	aosmith MV50466-8 VH cycles 2735-2771.Wave	1000-7260 psi
2808	12/10/11	37	12-10-2011 37 cycles.Wave	1000-7260 psi
2856	12/11/11	48	12-11-2011 48 cycles.Wave	1000-7260 psi
2906	12/12/11	50	12-12-2011 50 cycles.Wave	1000-7260 psi
2957	12/13/11	51	12-13-2011 51 cycles.Wave	1000-7260 psi
3003	12/14/11	46	12-14-2011 46 cycles.Wave	1000-7260 psi
3049	12/15/11	46	12-15-2011 46 cycles.Wave	1000-7260 psi
3092	12/16/11	43	12-16-2011 43 cycles.Wave	1000-7260 psi
3137	12/17/11	45	12-17-2011 45 cycles.Wave	1000-7260 psi
3183	12/18/11	46	12-18-2011 46 cycles.Wave	1000-7260 psi
3210	12/19/11	27	12-19-2011 27 cycles.Wave	1000-7260 psi
3211	12/19/11	1	12-19-2011 1 cycle 7920 psi.Wave	0-7920 psi
3253	12/20/11	42	12-20-2011 42 cycles.Wave	1000-7920 psi
3292	12/21/11	39	12-21-2011 39 cycles.Wave	1000-7920 psi, new sensor locations
3328	12/22/11	36	12-22-2011 36 cycles.Wave	1000-7920 psi
3363	12/23/11	35	12-23-2011 35 cycles.Wave	1000-7920 psi
3402	12/24/11	39	12-24-2011 39 cycles.Wave	1000-7920 psi
3448	12/25/11	46	12-25-2011 46 cycles.Wave	1000-7920 psi
3494	12/26/11	46	12-26-2011 46 cycles.Wave	1000-7920 psi
3520	12/27/11	26	12-27-2011 26 cycles.Wave	1000-7920 psi
3551	12/28/11	31	12-28-2011 26 cycles.Wave	1000-8400 psi
3584	12/29/11	33	12-29-2011 26 cycles.Wave	1000-8400 psi
3615	12/30/11	31	12-30-2011 26 cycles.Wave	1000-8400 psi
3646	12/31/11	31	12-31-2011 26 cycles.Wave	1000-8400 psi
3673	1/1/12	27	1-1-2012 27 cycles.Wave	1000-8400 psi
3699	1/2/12	26	1-2-2012 26 cycles.Wave	1000-8400 psi
3728	1/3/12	29	1-3-2012 29 cycles.Wave	100-8400 psi
3756	1/4/12	28	1-4-2012 28 cycles.Wave	1000-8400 psi
3782	1/5/12	26	1-5-2012 26 cycles.Wave	1000-8400 psi
3804	1/6/12	22	1-6-2012 22 cycles.Wave	1000-8400 psi. Drilled holes in long seam weld and in outer wrap
3832	1/7/12	28	1-7-2012 28 cycles	1000-8400 psi
3858	1/8/12	26	1-8-2012 26 cycles	1000-8400 psi
3884	1/9/12	26	1-9-2012 26 cycles	1000-8400 psi. Drilled starter holes/scored holes in long seam weld and wrap
3910	1/10/12	26	1-10-2012 26 cycles	1000-8400 psi
3936	1/11/12	26	1-11-2012 26 cycles	1000-8400 psi
3951	1/12/12	15	1-12-2012 15 cycles	1000-8400 psi. Pump died
3994	1/20/12	43	1-20-2012 43 cycles	1000-6600 psi cycles
4046	1/21/12	52	1-21-2012 52 cycles	1000-8400 psi cycles from now on
4100	1/22/12	54	1-22-2012 54 cycles	1000-8400 psi
4144	1/23/12	44	1-23-2012 44 cycles	1000-8400 psi
4187	1/24/12	43	1-24-2012 43 cycles	1000-8400 psi
4231	1/25/2012	44	1-25-2012 44 cycles	1000-8400 psi
4238	1/26/2012	7	1-26-2012 7 cycles	1000-8400 psi. Pump died
4286	1/27/2012	48	1-27-2012 48 cycles	1000-8400 psi
4342	1/28/2012	56	1-28-2012 56 cycles	1000-8400 psi
4395	1/30/2012	53	1-30-2012 53 cycles	1000-8400 psi

4431	1/31/2012	36	1-31-2012 36 cycles	1000-8400 psi
4486	2/2/2012	55	2-2-2012 55 cycles	1000-8400 psi
4530	2/3/2012	44	2-3-2012 44 cycles	1000-8400 psi
4535	2/4/2012	5	2-5-2012 5 cycles	1000-8400 psi
4548	2/21/2012	13	2-21-2012 13 cycles	new pump, 2000-8400 psi cycles
4560	2/22/2012	12	2-22-2012 12 cycles	2000-9500 psi cycles
4561	2/22/2012	1	2-22-2012 1 cycles	first 10,000 psi cycle - strain not turned on in pressure software so stopped test
4573	2/23/2012	12	2-23-2012 23 cycles	2000-10,000 psi cycles
4583	2/24/2012	10	2-24-2012 10 cycles	2000-10,000 psi cycles
4603	2/26/2012	20	2-26-2012 20 cycles	2000-10,000 psi cycles
4617	2/27/2012	14	2-27-2012 14 cycles	2000-10,000 psi cycles
4639	3/3/2012	22	3-3-2012 22 cycles	2000-10,000 psi. Pressure transducer changed from 10,000 psi/10 v to 30,000 psi/10 v, WE software not changed
4661	3/5/2012	22	3-5-2012 22 cycles	
4662	3/5/2012	1	3-5-2012 1 cycles	14,000 psi run. Correction in We software for voltage conversion made
4683	3/7/2012	21	3-7-2012 21 cycles	2000-10,000 psi cycles
4688	3/8/2012	5	3-8-2012 5 cycles	6000-14,000 psi cycles

Appendix B. Modal Acoustic Emission Detection Sensitivity

Theoretical Calculation of Modal Acoustic Emission Sensor Spacing Using Fracture Mechanics

Since the early 1980's, acoustic emission (AE) has been used for the examination of seamless steel tubes used in tube trailers (high strength modified AISI 4130 and 4140). Blackburn and Rana [1] used fracture mechanics to determine the maximum permissible existing flaw sizes that were required to be found by AE detection and ultrasonic inspection (UT) measurement based on the mandatory DOT 5-year inspection interval to ensure that an existing flaw would not grow to critical size between inspections. Based on this work, an ASTM standard, E 1419, *Standard Test Method for Examination of Seamless, Gas-Filled, Pressure Vessels using Acoustic Emission*, was written that outlines the steps in examining seamless tubes using the AE equipment that was commercially available at the time.

While this work gave a fracture mechanics basis for the flaw size detectability requirement so that a flaw would not grow to a critical size before the specified examination interval, it gave no guidance on the AE detectability, e.g., sensor spacing and energy release (amount of incremental crack extension area) that could be detected for a given material. It gave a standard sensor placement, instrument settings and sensor response which were based on empirical knowledge at the time, and correlated the AE findings to UT flaw characterization measurements with good results. Significantly, it required the use of UT examination to characterize the emission sources, which is problematic for many vessel configurations, including tube trailers. The ASTM E 1419 standard is being extended by testers to other pressure vessel configurations and materials (e.g., stainless steel tanks) for which this test method may or may not be valid. For this standard to be extended to other types of vessels and materials a fracture mechanics based analysis of the vessel material, design and flaw geometry must be developed to determine the required sensitivity of the system. Using these calculations, the examiner can set the correct sensitivity of the system, either by increasing system gain or increasing the number of transducers used, so that a valid test can be performed.

The ability to perform AE testing by capturing and evaluating individual acoustic wave modes using broadband sensors was developed in the late 1980's. Modal Acoustic Emission (MAE) lends itself to the detection, identification and fracture mechanics analysis for flaw detection. The wave mode identification capabilities of MAE has resulted in the ability to sort noise events from true flaw growth events, eliminating the problem associated with conventional AE of false positives due to the non-independent variable analysis [2-4]. The energy calculations required for a fracture mechanics analysis can easily be performed on the digitized waveforms captured using MAE as well. This paper presents an approach using fracture mechanics analysis to predict the energy release due to cyclic fatigue in 4130X steel. Data from flaw growth in a seamless steel pressure vessel is then compared to the theoretical fracture mechanics calculations to determine if the method can be used to aid in determining system sensitivities, e.g., sensor spacing, for flaw growth detection.

Waveform Capture and Analysis

A short discussion of data capture is presented here. Modal acoustic emission requires the use of a broadband system to properly capture the surface displacement from the propagating wave for

analysis. The strength of the analysis is that it does not rely on empirical relationships between parameters such as counts, amplitude, energy and duration. Parameters such as these are not independent (e.g., higher amplitude means greater energy, longer duration and more counts). Secondly, wave propagation effects, such as geometric attenuation, are not accounted for in parameter based AE, e.g., an event detected at two different distances from the source, will have two different energies, even though the source was the same. Thus, distribution plots, such as energy, amplitude, and duration will not take the attenuation into account, and are often seen as meaningless [5]. Using MAE eliminates these issues since the wave propagation analysis accounts for these effects. This paper will not cover the science of wave propagation in thin walled media, and the reader is directed to the many readily available references in this subject.

Fracture Mechanics Energy Analysis for Crack Growth

The focus of this paper is to develop a theoretical basis for determining the detectability of crack growth using MAE. From ASTM 1419, the system threshold for an examination using that standard is 32 dB_{AE}. For most systems, this requirement is near the noise floor of the electronics, and no further sensitivity can be achieved by increasing the gain, or amplification, of the system. Many systems apply a narrow band filter to the signals to reduce noise, but when this is done, wave mode information is lost, and the ability to sort noise signals from flaw growth signals is lost as well. This results in false positives, and perfectly good pressure vessels either failing the examination, or inspector dispositions that require the use of follow up NDE – dispositions that are either not acceptable or helpful when follow up NDE is not feasible, e.g multi-layered pressure vessels. MAE overcomes this by identifying relevant, flaw based emissions, which can be evaluated on the basis of actual energy content. This section outlines the steps required to calculate the energy release due to crack growth in a given material and structural geometry due to cyclic fatigue. This value is then used to determine the sensor spacing required to detect crack growth.

Step 1. Theoretical energy released by cyclic fatigue crack growth

The first step in determining if crack growth in a given material is detectable is to calculate the theoretical energy release rate, *G*, of the material for Mode I crack growth. From [6],

$$G = \frac{K_I^2}{E}\left(1-\nu^2\right)$$

Where *G* (units of lb/in) is the energy release rate, i.e., rate of change in potential energy with the crack area (a.k.a., crack extension force and crack driving force, K_I is the Mode I stress intensity factor for the given geometry, *E* is Young's modulus, and ν is Poisson's ratio. If these values are known for a given material, the energy release rate can be calculated. When this value is multiplied by the crack growth area, the total theoretical energy released by the crack growth is calculated. However, when this is calculated for a material such as steel, the energy is much greater than the energy calculated from a waveform captured due to flaw growth. The reasons for this are discussed in detail in the following sections, but a quick overview is provided below.

1. Most of the energy from crack growth is released due to free surface formation of the crack, and very little of the energy is transformed into wave propagation.
2. The sensor only captures the wave displacement directly under its face. As the wave propagates away from the source, the sensor only detects a very small portion of the wave energy.

The following steps describe how to account for the effects described above.

Step 2. Theoretical Cyclic fatigue crack growth

The second step in determining system sensitivity is to calculate the theoretical crack growth per fatigue cycle for a given material and crack configuration. This is typically done by integrating the da/dN curve for a given material from experimental data. The data used in this paper was for a DOT 4301X specification steel. Reference [1] gives the Fatigue crack growth (FCG) rate equation for this steel:

$$\frac{da}{dN} = \left(0.66\times10^{-8}\right)\left(\Delta K_I\right)^{2.25}, \quad \text{at } R=0,$$

where:

$$K_I = M\sigma\sqrt{\frac{\pi a}{Q}}$$

K_I is the stress intensity factor, M is the correction factor for membrane stress, Q is the flaw shape parameter and a is the crack depth. For this work, Q=1.0.

When integrated, this gives the following equation for the amount of crack growth per cycle as:

$$a_f = \left[\frac{1}{a_i^{-0.125} - (0.125)(0.66\times10^{-8})(M^{2.25}\Delta\sigma^{2.25}\pi^{1.125}\Delta N)}\right]^8$$

Where a_i is the initial crack size, a_f is the final crack growth, and $\Delta\sigma$ is the difference between the maximum and minimum cyclic stress.

In reference [1], the value used for M was 1.5 and the cyclic stress to which the test cylinder was subjected was 34 ksi. Plotting this equation using an initial crack depth of 0.1 inches (about ¼ critical size at the specified conditions) results in the following plot, Figure A-1.

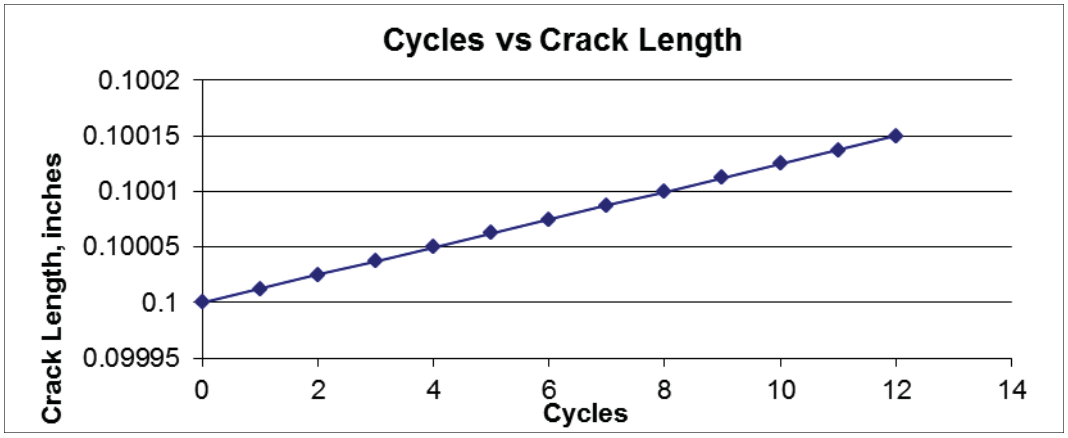

Figure A-1. Crack growth per cycle for 3AAX steel.

The plot in Figure A-1 is for the initial crack growth, and results in a conservative crack extension per cycle of approximately 0.00001 inches per cycle with an applied membrane stress of 34 ksi.

It is noted that these results are for incremental fatigue crack growth behavior and not for ductile tearing that would occur during rapid fracture near critical, end of life crack growth.

Step 3. Calculation of the detected energy at the transducer
The next step is to determine how much of the energy of the propagating wave created by crack opening is detected at the AE transducer. As the wave propagates, it spreads out in a ring. As it propagates further from the source, there is less energy per unit length since the circumference of the wave front is expanding while the total energy remains constant. This effect is known as geometric dispersion. The fraction of wave energy that the sensor detects is due to this effect is:

$$Energy_{Wave} = \frac{D_{Sensor}}{2\pi R}$$

Where $Energy_{Wave}$ is the fraction of wave energy detected, D_{Sensor} is the diameter of the sensor, and $2\pi R$ is the circumference of the wave front due to the distance of the sensor from the source, R. For a source 10 feet from a 0.5 inch diameter transducer, this would result in approximately 0.0007 of the total wave energy being detected by the sensor.

Step 4. Calculation of energy converted to wave motion
Reference [7] discusses in detail the experimental method used to measure the energy conversion from G, the energy release rate, to G_{MAE}, the energy release rate in the modal acoustic emission (MAE) wave. A short summation is provided here.

A sensor is coupled to an aluminum plate (7075-T6) of given dimensions [7]. To impart a known energy into the plate, an incline of known length and height is placed against the edge of the aluminum plate. The height of the incline is adjusted so a ball of known diameter impacts the edge of the plate normally, at the centerline of the plate and at the centerline of the ball. The transducer is placed a known distance away from the point of impact and acoustically coupled to the plate. The energy of the rolling ball impact (RBI) can be calculated using $E = mgh$. The resulting waveform from the impact is captured using a high speed digitizer, and the energy in the first half cycle of the extensional mode calculated by integrating V^2 over time, as shown in the equation below, and then dividing by the input impedance to the preamplifier.

$$U = \int_0^T V^2 dt / Z$$

Where U is the wave energy, in Joules, V is the signal amplitude in volts and Z is the impedance at the preamplifier in Ohms.

The scaling factor is then calculated by dividing the wave energy by the energy of the rolling ball impact, mgh. For the electronics and sensor used for this testing, this scaling factor was calculated to be 2.63×10^{-7}. From this number it can be seen that the amount of energy released in the form of a propagating wave is very small compared to the initiating event. The correspondingly much smaller energy released and detected from creation of a typical free crack surface is determined below.

Step 5. Determining theoretical crack growth detectability from cyclic crack growth
The final step is to take the information from Steps 1-4, and calculate the energy of the wave from the cyclic fatigue crack growth to determine the theoretical sensor spacing required for crack growth detection. The steps are:

1. Calculate G for the given material
2. Multiply G by the wave scaling factor to get G_{MAE}
3. Calculate the geometric attenuation factor for the distance of propagation, $Energy_{Wave}$ and multiply G_{MAE} by this factor to get G_{MAE}^{Attn} to get the fully scaled energy release for both the wave energy and the geometric attenuation energy
4. Multiply G_{MAE}^{Attn} by the crack growth area, A to get the total energy released by the crack growth that results in wave propagation.

Example for 4130X steel for theoretical crack growth wave energy release
Assumed values for calculations
σ = 34 ksi
a = 0.1 in
ν = 0.3
E = 30x10^6 psi
Propagation Distance = 50 inches
Sensor Diameter = 0.25 inches
G_{MAE} scaling Factor = 2.63x10^{-7}
To calculate G, the following equation from reference [6] is used:

$$G = \frac{K_I^2}{E}\left(1-\nu^2\right); \qquad K_I = 1.12\sigma\sqrt{\pi\frac{a}{Q}} \bullet M_K$$

From [6], K_I is the stress intensity factor for a part through crack in a plate. M_K is approximately 1.0 for the crack geometry in this example, Q = 1.1.

Using the above values and equations, the following values were calculated:

Geometric Attenuation Correction for 50 inches = 0.25 in/(2πx50 in) = 0.0008

K_I = 20.35 (ksi)(in)$^{1/2}$

G = 12.6 lb/in

G_{MAE} = G x 2.63x10^{-7} = 3.31x10^{-6} lb/in

G_{MAE}^{Attn} = G_{MAE} x $Energy_{Wave}$ = 3.31x10^{-6} lb/in x .0008 = 2.65x10^{-9} lb/in

To calculate the amount of crack growth area, A, the following rationale was used. Shown in Figure A-2 is a schematic of an elliptical crack in the sidewall of a pressure vessel. The assumption is a 4:1 ratio for c to a, from reference [1]. The figure shows the initial crack (dotted line) and the crack after it has grown a distance Δa, due to a fatigue cycle. If the initial value of a is 0.1 inches, then c is 0.4 inches. From the crack growth per cycle calculation, Figure A-2, Δa is 0.00001 inches, so then Δc must be 0.00004 inches to maintain the 4:1 aspect ratio. From

prior testing experience, the MAE source location shows that typically only one side of the notch grows during fatigue testing, not the entire length of the elliptical notch. Therefore, to calculate the area of crack growth, the area of the initial full ellipse (if it were an embedded flaw) is calculated from $A=\pi ac$, and the area of the crack growth full ellipse is calculated, $A=\pi(a+\Delta a)(c+\Delta c)$, and the two areas subtracted to get the difference in areas, ΔA. The ΔA is then divided by four to get the area of one side of the notch growth. The squares in Figure A-2 below show the proposed area of crack growth. Doing these calculations results in an increase in notch area of 6.3×10^{-6} in^2, due to a crack depth increase of 0.00001 inches.

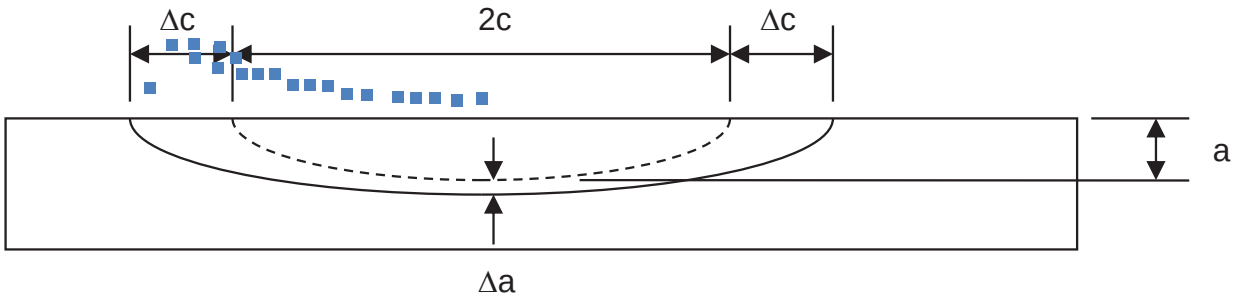

Figure A-2. Schematic of crack growth.

Using these values, the theoretical corrected wave energy release is:
$G_{MAE}^{Attn} \times A = (2.65 \times 10^{-9}$ lb/in)(6.3×10^{-6} in^2)(1/12 ft/in)(1.356 J/ft lb) = 1.89×10^{-15} Joules
This energy is the baseline energy for cyclic flaw growth in 4130X steel at the stated conditions. This number will be used to set the system sensitivity for crack growth detection.

Experimental Modal Acoustic Emission Data

A waveform from crack growth in a pressure vessel manufactured from 4130X steel is shown in Figure A-3. The data shown was from a test performed to the ASTM E 1419 standard where two sensors were acoustically mounted to the tube, approximately 400 inches apart, and the vessel pressurized to 110% of operating pressure. The source of the waveform was located approximately 50 inches from sensor 1, and 350 inches from sensor 2. The location of the flaw was verified with follow up ultrasonic inspection. The system gain was set to 68 dB (x2511).

Using the waveforms in Figure A-3, the energy contained in the signal can be calculated. Only the energy of the direct wave is used (reflections are not included in the calculation, as that would add energy that was not in the initial source). The signal between the vertical bars on each signal was used for the energy calculation. The voltage for each digitized point was squared, multiplied by the 1/sampling rate, divided by the gain squared (2511^2), and then divided by the input impedance of the preamplifier (10,000 Ω). This gave an energy value for Channel 1 of 8×10^{-16} J, and for Channel 2, 1.28×10^{-16} J.

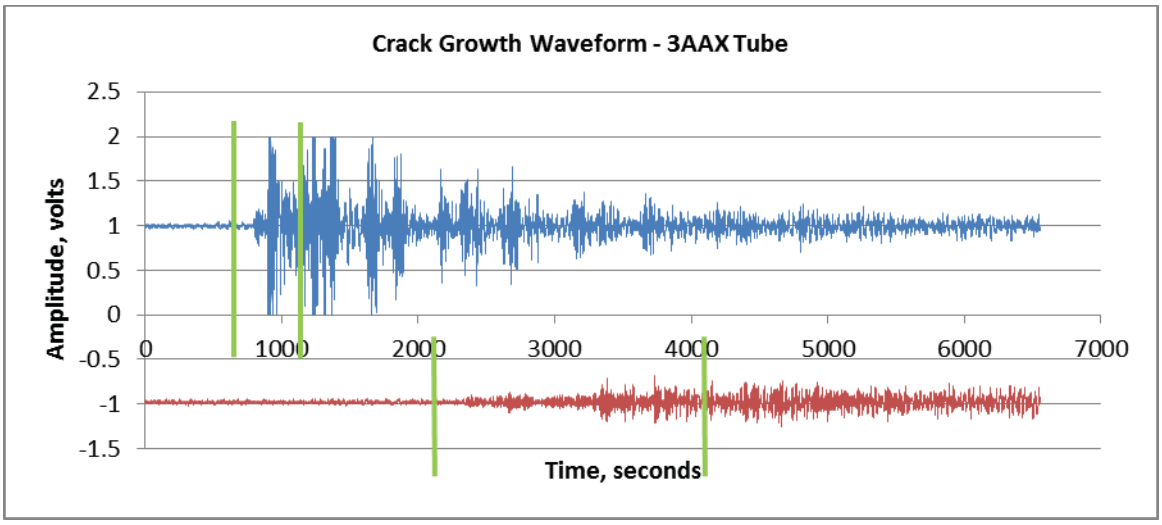

Figure A-3. Crack growth signal from a 3AAX tube. The waveform from channel 1 is shown in blue, and channel 2 is shown in red.

A greater signal length was used for sensor 2 due to the dispersion of the wave as it propagated a longer distance. The amount of propagation time for the lower frequencies contained in the flexural mode of the signal was calculated from the dispersion curve for this material to be about 3300 μseconds (using a propagation velocity of 106,000 in/sec). Adding this to the initial trigger point in sensor 1 of approximately 800 μseconds, gave a time of 4100 μseconds for the arrival of the lower frequencies in the flexural mode that travel at much slower velocities than those in the extensional mode.

If we compare the theoretically calculated energy values to the experimentally determined values for each channel, we have the following results shown in Table A-1.

Table A-1. Theoretical calculated and experimentally measured wave energy.

	Theory	**Experiment**	**% Difference**
Ch 1 Energy – 50”	$1.89e^{-15}$ J	$8.0e^{-16}$ J	42
Ch 2 Energy – 350”	$2.67e^{-16}$ J	$1.28e^{-16}$ J	48

This result is well within experimental error for these types of calculations, and likely can be improved with better sensor calibration measurements and fracture mechanics values. Most likely, the largest error in the calculation is the theoretical crack growth area, since that is the greatest unknown in the measurement.

Usage of waveform energy release in MAE testing to determine sensor spacing

Sensor spacing in acoustic emission and MAE testing has been based on testing experience and development of empirical standards. ASME E 1118, *Acoustic Emission Examination of Reinforced Thermosetting Resin Pipe (RTRP)*, has a sensor spacing requirement based on attenuation of signals in a lead plate. While this provides the novice examiner with a guideline, it is impractical to carry a lead plate of the required dimensions to test sites.

The work in this paper allows the examiner to set conservative a sensor spacing that is based on fracture mechanics testing and material values for the material the vessel was manufactured from. The spacing should be on the conservative side since it is based on the cyclic fatigue of

the vessel at operating loads, and a much smaller initial crack size than what would be required for the flaw to reach critical crack size during the recertification period. MAE testing uses a 110% of operating overstress to exercise the crack in a structure. The increased pressure and a larger initial crack depth would result in a greater energy release, resulting in larger energy signals.

Figure A-4 shows a way that the fracture mechanics calculations could be used to develop sensor spacing curves for a given material. For a given crack growth area, the energy release is calculated, and then plotted for a sensor spacing. The Figure A-4 log-log plot shows the waveform energy (y-axis) and crack growth area (x-axis) plotted as a function of sensor distance from the source (colored lines), for the 4130X steel used in the example in this paper. Using steps 1-5 outlined previously in the paper, one can determine the proper sensor spacing for the data acquisition system used.

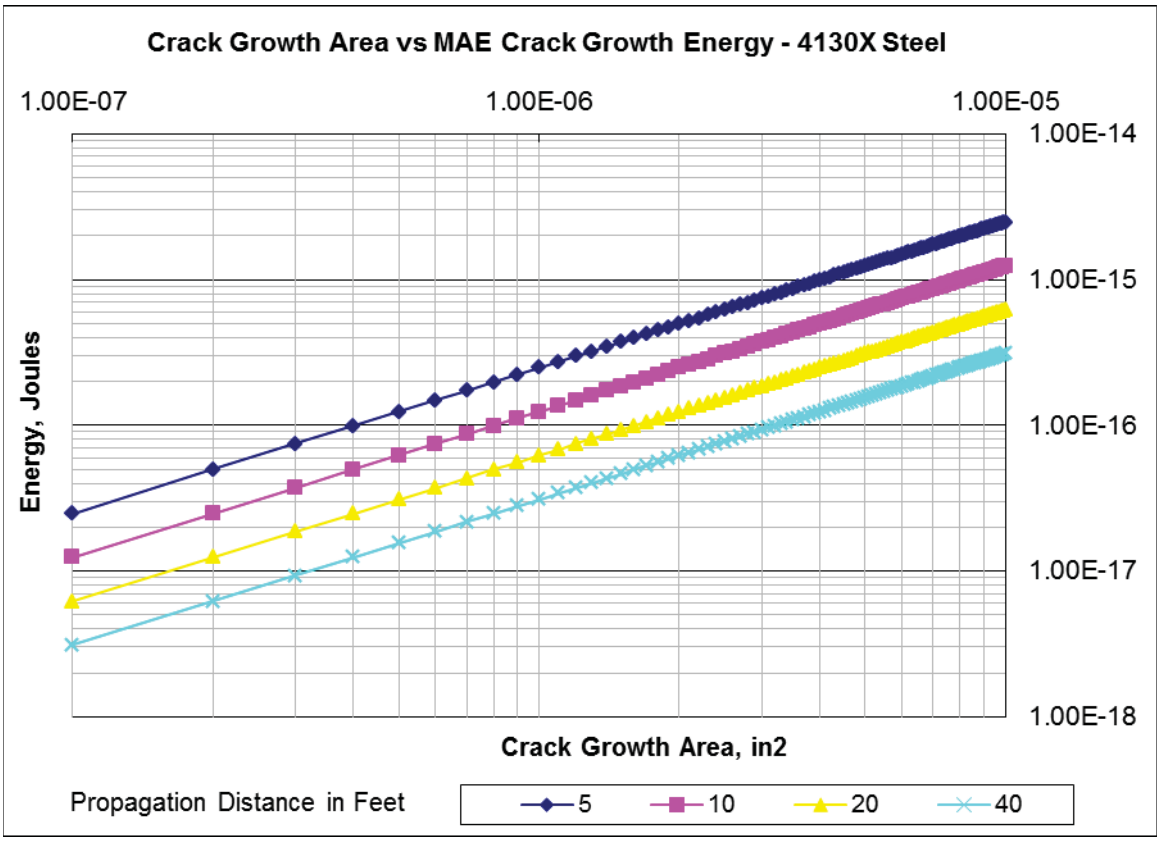

Figure A-4. Sensor spacing as a function of waveform energy (y-axis) and crack growth area.

For example, the energy noise floor for the system used in the experimental data is approximately $1x10^{17}$ J for a quiescent signal (no MAE signal in the data). If a rule of thumb of a signal-to-noise ratio of two is used to set the minimum signal sensitivity, this would result in a floor of $2x10^{-17}$ Joules. That would mean for our example, a crack growth area of $6.3x10^{-6}$ in^2 and an energy release of $1.89x10^{-15}$ Joules, that a sensor spacing of up to 40 feet could be used for the detection of signals of this size. Based on experience and data from 1.1 inch thick and 5/8 inch thick steel cylinders that have been MAE tested, this is typically the maximum distance

that can be reliably detected for cyclic flaw growth. Please note that the noise floor of the instrumentation must be measured to determine the minimum signal level detection.

Also note that, as previously mentioned, this detection capability is based on stable fatigue crack growth, not ductile tearing associated with near-critical rapid flaw growth. That regime is not addressed in this paper.

Discussion

While the theory presented in this paper is verified on a very limited sample of actual data, it does provide a baseline rationale for the placement of sensors when performing MAE testing. Sensitivity of the technique has always been an issue, and this analysis approach can provide insight to the sizing of flaw growth using MAE (i.e., what amount of crack growth is detectable) – note that this is different from determining the physical size of the flaw. Flaw size, or depth, is answered not by this work, but by observing the extensional and flexural mode amplitudes to determine approximate crack depth [3], or by using a secondary inspection method, such as ultrasound, when possible.

Obviously, actual fracture/waveform data is needed to fully verify and validate this approach, but it is based on science and well established plate wave propagation characteristics, and for metallic materials that have well documented fracture mechanics material data associated with them, this gives the examiner and owner a framework for helping to ensure that the testing is valid and the parameters that are being measured meet the intended goals of the test.

Furthermore, the fracture mechanics analysis will rule out the use of acoustic emission testing on materials that will not have enough energy release to create detectable events, e.g., low strength stainless steel vessels.

Conclusions

A method has been presented to theoretically calculate the energy released due to crack growth in 4130X steel as it relates to acoustic wave detection and assessment. The purpose of the method is to provide examiners using modal acoustic emission a science based method to assist in determining maximum sensor spacing to ensure that crack growth signals can be reliably detected on their equipment. The theoretical calculations were compared to crack growth data in a single wall forged pressure vessel manufactured from 4130X steel. The results were:

1. An approach that correlates the energy release calculated using fracture mechanics to the energy contained in captured modal acoustic waveforms has been developed.
2. The calculated energy from fracture mechanics can be used to develop maximum sensor spacing limitations for MAE sensors to ensure that relevant flaw growth is detected.

This approach should allow the extension of acoustic emission testing standards such as ASTM E 1419 to other materials and give the examiner confidence that the sensitivity of the system is meeting the test objectives.

References

1 Blackburn, P.R., Rana, M.D., “Acoustic Emission Testing and Structural Evaluation of Seamless, Steel Tubes in Compressed Gas Service,” *Journal of Pressure Vessel Technology*, May 1986, vol. 108, pp. 234-240.

2 Gorman, M.R., “Plate Wave Acoustic Emission,” *Journal of the Acoustical Society of America*, 1991, vol. 90, no. 1, pp. 358-365.
3 Gorman, M.R., Prosser, W.H., “AE Source Orientation by Plate Wave Analysis,” *Journal of Acoustic Emission*, 1991, vol. 9, no. 4, 283-288.
4 Ziola, S.M., “Digital Signal Processing of Modal Acoustic Emission Signals,” Journal of Acoustic Emission, 1996, vol. 14, no. 3-4, pp. S12-S18.
5 Goransen, “Jet Transport Structures Performance Monitoring,” *Structural Health Monitoring, Current Status and Perspectives*, Proceedings of the International Workshop on Structural Health Monitoring, Stanford University, CA, September 18-20, 1997.
6 Barsom, J.M., Rolfe, S. T., “Fracture and Fatigue Control in Structures, Applications of Fracture Mechanics,” Second Edition, Prentice-Hall, 1987.
7 Gorman, M.R., “Modal AE Analysis of Fracture and Failure in Composite Materials, and the Quality and Life of High Pressure Composite Pressure Vessels,” *Journal of Acoustic Emission*, 2011, vol. 29, pp. 1-28.

Appendix C. WaveExplorer™ Digital Filter Settings

These are the digital filter settings used in the software for the data analysis.

Filter	Qualifier	Value	Number of Channels to Pass On
Threshold	≥	100 mV	0
Parametric	≥	2.5 volts	NA
Pretrigger (PTE)	≤	0.4 V^2-msec	16
Saturation (Satur.)	≤	1	%
Confidence (Conf.)	≥	10	%
Energy	≥	4 V^2-msec	4
Frequency (Freq)	≥	15 kHz	NA

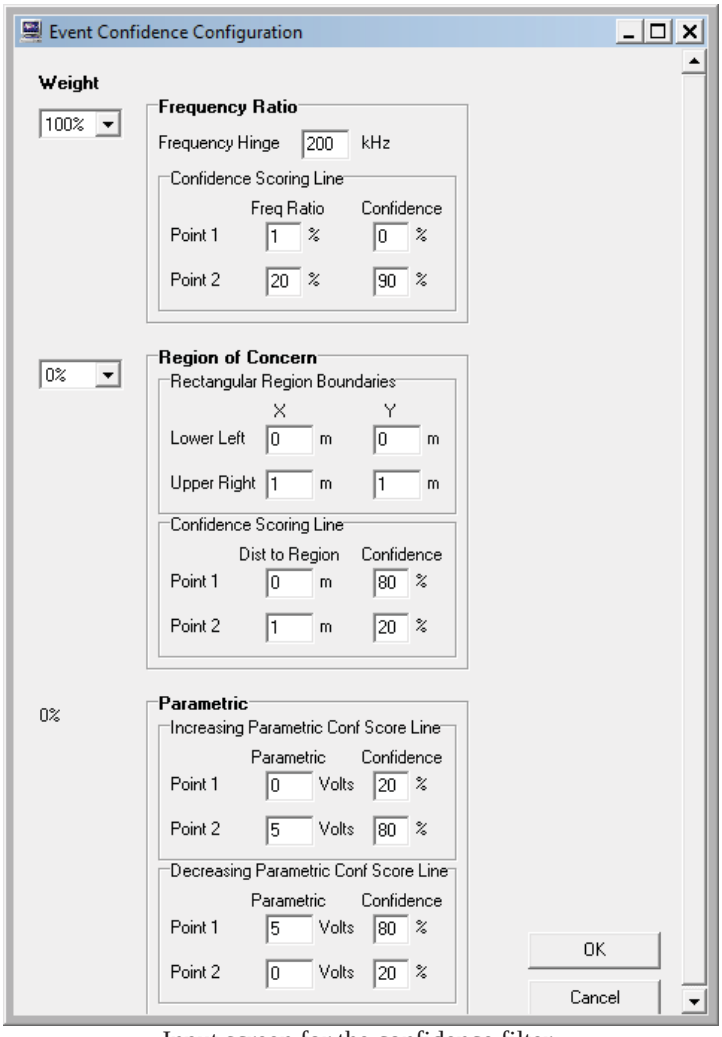

Input screen for the confidence filter.

REPORT DOCUMENTATION PAGE

Form Approved
OMB No. 0704-0188

1. REPORT DATE *(DD-MM-YYYY)*	2. REPORT TYPE	3. DATES COVERED *(From - To)*
01- 01 - 2014	Contractor Report	

4. TITLE AND SUBTITLE
Cyclic Crack Growth Testing of an A.O. Smith Multilayer Pressure Vessel with Modal Acoustic Emission Monitoring and Data Assessment

5a. CONTRACT NUMBER
NNA09DB39C

5b. GRANT NUMBER

5c. PROGRAM ELEMENT NUMBER

6. AUTHOR(S)
Ziola, Steven M.

5d. PROJECT NUMBER
OSMA SMA Project 724297

5e. TASK NUMBER

5f. WORK UNIT NUMBER
724297.20.21.01.03

7. PERFORMING ORGANIZATION NAME(S) AND ADDRESS(ES)
NASA Langley Research Center
Hampton, VA 23681-2199

8. PERFORMING ORGANIZATION REPORT NUMBER

9. SPONSORING/MONITORING AGENCY NAME(S) AND ADDRESS(ES)
National Aeronautics and Space Administration
Washington, DC 20546-0001

10. SPONSOR/MONITOR'S ACRONYM(S)
NASA

11. SPONSOR/MONITOR'S REPORT NUMBER(S)
NASA/CR-2014-218156

12. DISTRIBUTION/AVAILABILITY STATEMENT
Unclassified - Unlimited
Subject Category 39 Structural Mechanics
Availability: NASA CASI (443) 757-5802

13. SUPPLEMENTARY NOTES
Publication of this report was requested by the NESC. This task was funded by OSMA in with funds transferred to ARC for program execution. Doug Fraser was the NASA Project Manager at ARC. Jacobs ATOM managed the project through their contracts office under NASA contract NNA09DB39C. Owen Greulich and Doug Fraser were the NASA Technical Monitors.

14. ABSTRACT

Digital Wave Corp. (DWC) was retained by Jacobs ATOM at NASA Ames Research Center to perform cyclic pressure crack growth sensitivity testing on a multilayer pressure vessel instrumented with DWC's Modal Acoustic Emission (MAE) system, with captured wave analysis to be performed using DWCs WaveExplorerTM software, which has been used at Ames since 2001. The objectives were to document the ability to detect and characterize a known growing crack in such a vessel using only MAE, to establish the sensitivity of the equipment vs. crack size and / or relevance in a realistic field environment, and to obtain fracture toughness materials properties in follow up testing to enable accurate crack growth analysis. This report contains the results of the testing.

15. SUBJECT TERMS
Modal Acoustic Emission; Crack Growth Rate; Pencil Lead Break; Pressure Vessel

16. SECURITY CLASSIFICATION OF:			17. LIMITATION OF ABSTRACT	18. NUMBER OF PAGES	19a. NAME OF RESPONSIBLE PERSON
a. REPORT	b. ABSTRACT	c. THIS PAGE			STI Help Desk (email: help@sti.nasa.gov)
					19b. TELEPHONE NUMBER *(Include area code)*
U	U	U	UU	62	(443) 757-5802